NASA CR-156712

(NASA-CR-156712) FABRICATION AND TEST OF A VARIABLE CONDUCTANCE HEAT PIPE Final Report (Rockwell International Corp., Downey, Calif.) 78 p HC A05/MF A01 CSCL 20D

N78-19443

Unclas
G3/34 07353

SD 78-AP-0011

FABRICATION AND TEST OF A VARIABLE CONDUCTANCE HEAT PIPE

FINAL REPORT

NAS5-24171

JANUARY, 1978

Prepared by:

A. M. Lehtinen
Aerothermo
Advanced Programs

Approved:

A. Shimizu, Supervisor
Aerothermo
Advanced Programs

for J. J. Florey, Manager
Systems Design & Technology
Advanced Programs

Rockwell International
Space Division

FOREWORD

This report is submitted by Space Division of Rockwell International Corporation to the National Aeronautics and Space Administration, Goddard Space Flight Center in accordance with the requirements of Contract NAS5-24171. The work was administered by Mr. R. McIntosh, the Technical Monitor for Goddard Space Flight Center. The program was under the direction of A. M. Lehtinen, the Program Manager, and technical and laboratory assistance was provided by Messrs. J. P. Wright, C. D. Rosen and G. W. Gurr, Jr.

SUMMARY

Under Contract (No. NAS5-2417) for Goddard Space Flight Center (GSFC), a program was formulated for the design, fabrication and test of a variable conductance heat pipe (VCHP) with feedback control. The VCHP was fabricated with a reservoir-condenser volume ratio of 10 and an axially grooved action section. Fabrication was in accordance with established Space Division procedures for safe design, fabrication, and quality assurance procedures. Tests of the heat transport capability were greater than or equal to the analytical predictions for the no gas case. When gas was added, the pipe performance degraded by 18% at zero tilt as was expected. At .5 cm tilt, the performance degradation was 43%, which supports one hypothesis that a bubble occlusion existed in the evaporator grooves.

The placement of the reservoir heater and the test fixture cooling fins are believed to have caused a superheated vapor condition in the reservoir. Erroneously high reservoir temperature indications resulted from this condition. The observed temperature gradients in the reservoir lend support to this theory. The net result was higher than predicted reservoir temperatures. Also, significant increases in minimum heat load resulted for controller set point temperatures higher than 0°C.

The transient test showed that control within the tolerance band at 0°C was an attainable goal. At 30°C, control within the tolerance band was maintained, but high reservoir heater power was required. Analyses showed that control is not possible for reasonably low reservoir heater power. This is supported by the observation of a significant reservoir heat leak through the condenser. Also, this heat leak verified the analytical conclusion that the reservoir was slightly undersized.

CONTENTS

LIST OF ILLUSTRATIONS

1.0 INTRODUCTION

Precision thermal control using variable conductance heat pipes has been a major area of interest in design of reliable heat pipe thermal control systems. Under a contract with Goddard Space Flight Center (GSFC), a program was developed for the design, analysis, fabrication, and test of a variable conductance heat pipe. The program was undertaken to provide preliminary design data for the development of a thermal control canister, which is currently under development by Grumman.

A typical variable conductance heat pipe system with feedback control is shown in Figure 1-1. This type of system is often referred to as a feedback controlled heat pipe system (FCHP). Its basic components are: a heat transport section (evaporator, condenser, and adiabatic sections); a gas reservoir; and an electronic feedback controller. System control is maintained by the feedback controller comparing the temperature sensed at the control point with the desired controller set point temperature and then increasing or reducing heater power to the reservoir as required. This causes the gas front in the condenser section to reduce or increase heat rejection which will cause the control point temperature to seek the dialed controller set point temperature.

The design goals set in this program were a controller set point temperature range from 0°C to 30°C with $\pm$ 1°C tolerance. The environment to which the system is exposed varies from a maximum space sink temperature of -13°C to a minimum sink temperature of -120°C. The dissipated heat load is also variable, from the minimum power required to maintain the desired controller set point temperature to the maximum heat load which can be rejected from the radiator at the desired controller set point temperature. Also, the VCHP was designed to minimize the heat leak through the adiabatic section and to maintain a sharp gas front region in the condenser.

Finally, a test program was formulated to verify the VCHP performance. The three sets of tests used to verify the performance were the heat transport test, the steady state control tests, and the transient response tests. The analyses and tests of the VCHP ultimately resulted in design recommendations

and future areas of investigation.

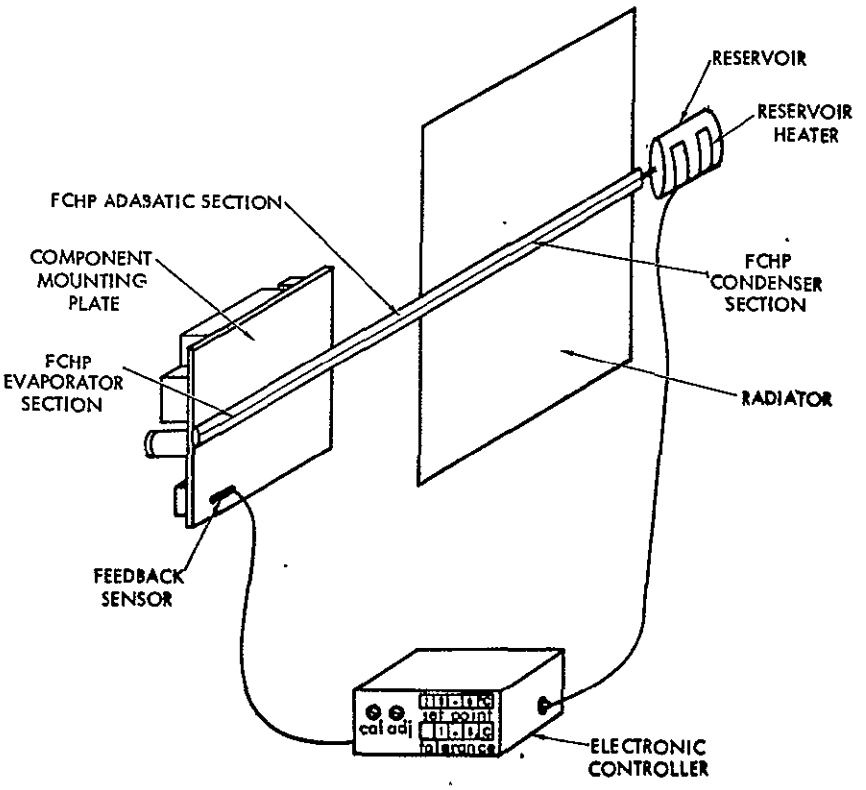

Figure 1-1 FCHP System

2.0 VCHP ANALYTICAL MODEL

The VCHP baseline design required that the evaporator section be 38.1 cm (15 in.), the adiabatic section be 30.5 cm (12 in.), and the condenser section be 76.2 cm (30 in.). In addition, the reservoir was manufactured from 316 stainless steel with a reservoir-to-condenser volume ratio of about 10:1. A 2-inch long stainless steel feeder tube with an aluminum-stainless transition joint was used to isolate the reservoir from the condenser. The adiabatic section of the pipe was machined to a .072 cm (.028 in.) wall thickness. Slots 1.27 cm (.5 in.) long were machined into the condenser with 2.54 cm flange interfaces between the slots (see detailed design drawings, Figure 4-1). The slots provide a sharper gas front for better VCHP control. This basic design data was used in a critical design analysis of the VCHP.

2.1 TRANSPORT CAPABILITY

Transport capability was determined on the Hewlett Packard 9820 system. The pressure balance equation is as follows.

$$1 + \frac{\Delta P_b}{\Delta P_c} = \frac{\Delta P_\ell}{\Delta P_c} + \frac{\Delta P_v}{\Delta P_c} + \frac{\Delta P_{\ell v}}{\Delta P_c} \qquad (2\text{-}1)$$

The liquid and vapor pressure drop calculations depend on the type of flow. Flow in the wick was assumed to be laminar, while vapor flow might be laminar, transitional, or turbulent. Defining the ratios of liquid and vapor pressure losses to capillary pressure rise in terms of heat transport results in the following relations.

$$\frac{\Delta P_\ell}{\Delta P_c} = \frac{\dot{Q}\, L_{eff}\, r_p}{2\, N_\ell\, K_\ell\, A_\ell\, \cos\,(\theta+\alpha)} \qquad (2\text{-}2)$$

$$\frac{\Delta P_v}{\Delta P_c} = \frac{\dot{Q} L_{eff}}{2N_\ell K_\ell A_\ell \cos(\theta+\alpha)} \left[\frac{\nu_v K_\ell A_\ell}{\nu_\ell D_{hv}^2 A_v} 2f_v \cdot Re_v\right] \quad (2\text{-}3)$$

The Reynolds number in these two equations can be defined in terms of heat transport as,

$$Re_v = \frac{\dot{Q} D_{hv}}{\lambda A_v \mu_v} = \frac{4\dot{Q}}{\lambda P_v \mu_v} \quad (2\text{-}4)$$

The Fanning friction factor used in equation 2-3 depends on the type of vapor flow. Therefore, the three flow regimes were defined in the following manner:

- Laminar flow; Re < 2000
- Transition flow; 2000 < Re < 3900
- Turbulen flow; Re > 3900

For each flow regime, the Fanning friction factor was defined by the following equations:

Laminar flow

$$f_v = \frac{16}{Re_v} \quad (2\text{-}5)$$

Transition flow

$$f_v = .009 + .001 \sin((Re - 2950)\,\pi/1900) \quad (2\text{-}6)$$

Turbulent flow

$$f_v = \frac{.079}{(Re_v)^{.25}} \quad (2\text{-}7)$$

In grooved heat pipes, another induced pressure drop becomes important. This pressure drop is due to the liquid-vapor shear interaction at the liquid surface. When the pressure drop is defined in terms of the capillary pressure rise and heat transport, the following equation results (References 3 and 12).

$$\frac{\Delta P_{\ell v}}{\Delta P_c} = \frac{\dot{Q}\, L_{eff}\, \omega_p}{2N_\ell\, K_\ell\, A_\ell \cos(\Theta+\alpha)} \frac{1}{6} \left[\frac{\nu_v}{\nu_\ell} \frac{(\omega/D_{hv})^2}{1 + \frac{s}{\omega}} \right] f_v \cdot Re_v \qquad (2\text{-}8)$$

Finally, the pressure drop due to body forces is given by

$$\frac{\Delta P_b}{\Delta P_c} = \frac{\rho_\ell\, g\, \frac{D\omega}{L} \sqrt{L^2 - h^2}\, r_p - \rho_\ell\, ghr_p}{2\sigma \cos(\Theta+\alpha)} \qquad (2\text{-}9)$$

In general, "g" is the acceleration due to earth gravity, although other accelerations could be used for specific situations.

When these equations are substituted into equation (2-1) and solved for the maximum heat transport, the following equations result.

$$\dot{Q}_{max} = \frac{2N_\ell\, K_\ell\, A_\ell\, (1+\eta) \cos(\Theta+\alpha)}{L_{eff}\, r_p\, (1 + V_v + L_v(R))} \qquad (2\text{-}10)$$

where

$$V_v = \frac{\nu_v}{\nu_\ell} \frac{K_\ell\, A_\ell}{D_v^2\, A_v} 2f_v \cdot Re_v$$

$$L_v = \frac{1}{6} \frac{\nu_v}{\nu_\ell} \frac{(\omega/D_{hv})^2}{1 + s/\omega} f_v \cdot Re_v$$

and R is an input variable for the liquid-vapor interaction pressure drop, input as a 1 or a zero depending on whether this term is applicable for the case of interest.

2.2 VCHP STEADY STATE CONTROL ANALYSIS

The steady state analysis utilized a modified flat front model which allows analysis of gas front entry into the adiabatic section. The assumed temperature profiles used in this technique are shown in Figure 2-1. These

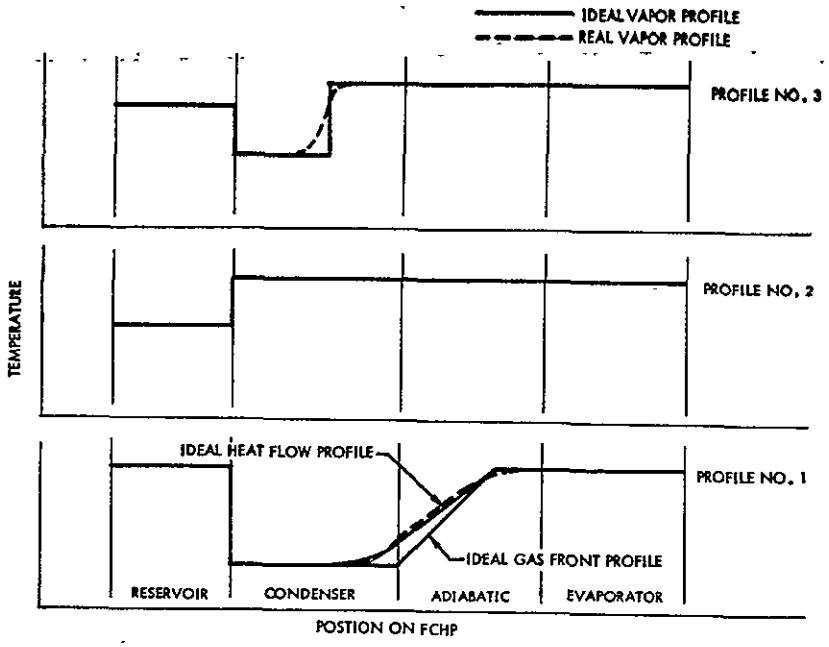

Figure 2-1 Vapor Temperature Profiles for FCHP Design Conditions

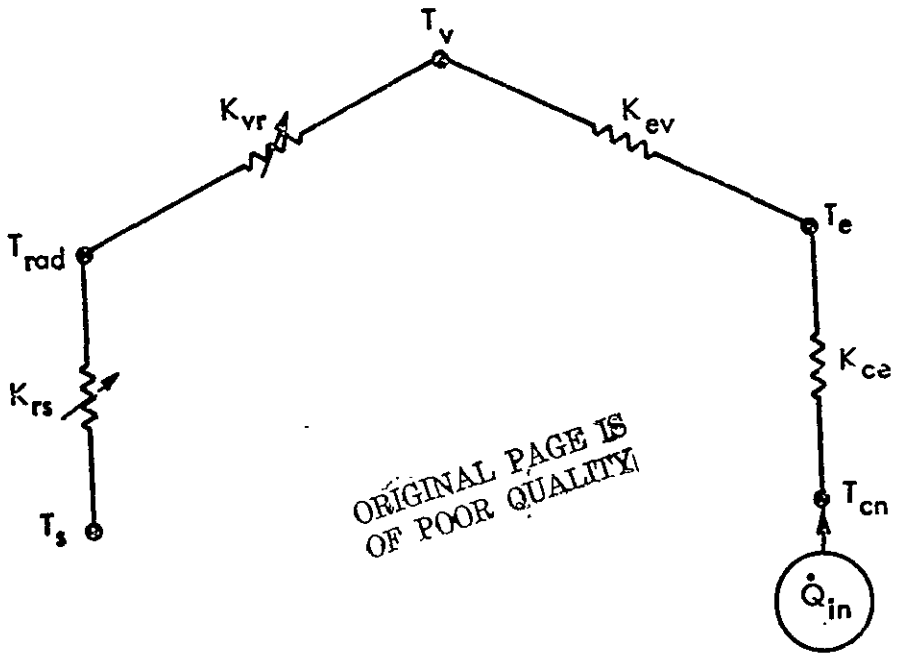

Figure 2-2 Thermal Network of FCHP System

profiles were used in the calculation of the heat flow and gas inventory. The dashed lines indicate what the real temperature profiles might look like. In a VCHP system, the real case will show a slight increase of the design set point temperature. In a FCHP system the predicted reservoir temperatures will be slightly higher than in the real case for the same controller set point temperature.

The second part of the model is the simple 5-node thermal network shown in Figure 2-2. This network is integrated with the assumed temperature profiles to calculate the temperature drops throughout the FCHP system.

A central concern to all analyses is the calculation of the vapor temperature. The calculations for the minimum and maximum vapor temperatures are made with respect to the minimum and maximum conditions. This results in the following general equations for the minimum and maximum vapor temperature.

$$T_{v\ min} = T_{cs} - \delta - \dot{Q}_{min}\left[\frac{1}{K_{ce}} + \frac{1}{K_{ev}}\right] \tag{2-11}$$

$$T_{v\ max} = T_{cs} + \delta - \dot{Q}_{max}\left[\frac{1}{K_{ce}} + \frac{1}{K_{ev}}\right] \tag{2-12}$$

T_{cs} is generally the controller set point temperature; but under the design set point condition, the design set point temperature is substituted. Unless otherwise stated, these equations will be used for vapor temperature determination in all the following analyses.

Control requires that the blockage length be determined for the worst case cold conditions. Under these conditions the VCHP is exposed to the minimum heat load, minimum sink temperature, and a control point temperature of $T_{set} - \delta$. For these conditions, it is necessary to determine if adiabatic gas blockage is required. To determine if the gas enters the adiabatic section, the following equations are solved to find the heat leak for full condenser blockage.

$$\dot{Q}_{div} = \eta_{rad}\ \varepsilon\ \sigma\ A_{rad} \left(T_{v\ div}^{\ 4} - T_{s\ min}^{\ 4} \right) \tag{2-13}$$

where

$$T_{v\ div} = T_{cs} - \delta - \dot{Q}_{div} \left[\frac{1}{K_{ce}} + \frac{1}{K_{ev}} \right] \tag{2-14}$$

For a minimum heat load less than $\dot{Q}_{div}$, adiabatic blockage occurs and the following equations calculates the required blockage length.

$$L_b = \frac{kA_{cs}}{\dot{Q}_{min}} \left(T_{v\ min} - T_{rad} \right) + L_c \tag{2-15}$$

For a minimum heat load greater than $\dot{Q}_{div}$, partial condenser blockage occurs and the following equations are used to find the blockage length..

$$f(\beta) = \dot{Q}_{min} - \eta_f\ \sigma\ \varepsilon\ A_{rad}\ (1 - \beta) \left[\left(T_{v\ min} - \frac{\dot{Q}_{min}}{hA\ L_c\ (1 - \beta)} \right)^4 - T_{s\ min}^{\ 4} \right] = 0 \tag{2-16}$$

where

$$\beta = L_b / L_c \tag{2-17}$$

Many of the following analyses will show β to be a convenient parameter for condenser blockage. Another convenient parameter for adiabatic blockage is α, which is defined as

$$\alpha = \frac{L_b - L_c}{L_a};\ \text{for } L_b \geq L_c \tag{2-18}$$

Two other relationships exist between α and β; these are

If $\beta < 1$; $\rightarrow \alpha = 0.0$

and

$$\text{If } \alpha \geq 0; \rightarrow \beta = 1.0$$

There are two set point temperatures of major concern. These are the design set point temperature and the controller set point temperature. The design set point temperature occurs when the worst case hot conditions are imposed and the reservoir temperature is at a minimum. Under this condition all of the gas is in the reservoir. The controller set point temperature is the temperature for which the ideal controller is set.

Under design set point temperature conditions, the FCHP system is exposed to the maximum heat load, maximum sink temperature, and minimum reservoir temperature. The radiator is full-on, the control point temperature is at $T_{ds} + \delta$, and the molar gas density in the reservoir is

$$\frac{n}{V_R} = \frac{P\left(T_{v\ max}\right) - P\left(T_{R\ min}\right)}{R\ T_{R\ min}} \tag{2-19}$$

A minimum reservoir volume is required for steady state thermal control of both the worst case hot and the worst case cold conditions. Generally, the reservoir volume required to maintain control is determined at a maximum controller set point temperature with the reservoir molar gas density determined at the design set point temperature. Analysis of the reservoir volume is also dependent on the restraints placed on the reservoir temperature.

When no reservoir temperature restraints are placed on the reservoir, the maximum reservoir temperature is allowed to approach the minimum vapor temperature. In this case, the required reservoir volume at a particular controller set point temperature is defined as follows:

$$\frac{V_R}{V_c} = \frac{\beta \dfrac{P\left\{T_{s\ min}\right\}}{T_{smin}} + \dfrac{2.0\ \alpha\ \phi}{T_{v\ min} + T_{s\ min}} P\left\{\dfrac{T_{v\ min} + T_{s\ min}}{2}\right\}}{R\ \dfrac{n}{V_R}} \tag{2-20}$$

where

$$P\left\{T_a\right\} = P\left(T_{v\ min}\right) - P\left(T_a\right)$$

Where maximum reservoir temperature restraints are present, then the following general control equation for the required reservoir volume is used:

$$\frac{V_R}{V_c} = \frac{\beta \dfrac{P_c\left\{T_{s\ min}\right\}}{T_{s\ min}} + \dfrac{2.0\ \alpha\ \phi}{T_{s\ min} + T_{v\ min}} P_a \left\{\dfrac{T_{s\ min} + T_{v\ min}}{2}\right\}}{\dfrac{n}{V_R} R \dfrac{P_R\left\{T_{R\ max}\right\}}{T_{R\ max}}} \qquad (2\text{-}21)$$

This equation is dependent on the maximum reservoir temperature only, but both maximum and minimum reservoir temperature have an effect on the controller set point temperature regime for which the solution of the equation is valid. That is, a minimum controller set point temperature can exist in theory if the minimum reservoir temperature is restrained to a temperature above the reservoir temperature at the design set point temperature.

Before the controller set point temperature regimes can be defined, the effect that the reservoir volume has on the maximum and minimum reservoir temperature must be determined. For finite reservoir volumes, the maximum and minimum reservoir temperature requirements are determined for a specified design set point temperature and a specified controller set point temperature. Parametric values of maximum reservoir temperature as a function of reservoir volume can be generated by the following equations.

$$P\left\{T_{R\ max}\right\} = P\left\{T_{v\ min}\right\} - \frac{\psi}{V_R/V_c} T_{R\ max} \qquad (2\text{-}22)$$

$$T_{v\ min} = T_{cs} - \delta - \dot{Q}_{min}\left[\frac{1}{K_{ce}} + \frac{1}{K_{ev}}\right] \qquad (2\text{-}23)$$

where

$$\psi = \frac{n}{V_R}\frac{V_R}{V_c} - \beta \frac{P\left(T_{v\ min}\right) - P\left(T_{s\ min}\right)}{T_{s\ min}} - \frac{2\ \alpha\ \phi}{T_{v\ min} + T_{s\ min}}\left[P\left(T_{v\ min}\right)\right.$$

$$\left. - P\left(\frac{T_{v\ min} + T_{s\ min}}{2}\right)\right] \qquad (2\text{-}24)$$

Parametric values of minimum reservoir temperature as a function of reservoir volume are generated by the following equations:

$$P\left\{T_{R\ min}\right\} = P\left\{T_{v\ max}\right\} - \frac{\psi'}{V_R/V_c} T_{R\ min} \qquad (2\text{-}25)$$

$$T_{v\ max} = T_{cs} + \delta - \dot{Q}_{max}\left[\frac{1}{K_{ce}} + \frac{1}{K_{ev}}\right] \qquad (2\text{-}26)$$

where

$$\psi' = \frac{n}{V_R}\frac{V_R}{V_c} R - \beta' \frac{P\left(T_{v\ max}\right) - P\left(T_{s\ max}\right)}{T_{s\ max}} - \frac{2\ \alpha'\ \phi}{T_{v\ max} + T_{s\ max}}\left[P\left(T_{v\ max}\right)\right.$$

$$\left. - P\left(\frac{T_{v\ max} + T_{s\ max}}{2}\right)\right] \qquad (2\text{-}27)$$

If reservoir temperature restraints exist, then the controller set point temperature will be further limited. The minimum reservoir temperature defines the lower limit of the control regime, and the maximum reservoir temperature defines the upper limit. These lower and upper limits are the minimum and maximum controller set point temperatures.

The minimum controller set point temperature is generally the design set point temperature, except when the minimum reservoir temperature is higher than reservoir temperature at the design set point. The equations for defining the minimum controller set point temperature are equations 2-25, 2-26, and 2-27 with the following substitution for V_R/V_c.

$$\frac{V_R}{V_c} = \left.\frac{V_R}{V_c}\right|_{min} = \frac{\beta \left\{ \frac{P \left\{T_{s\ min}\right\}}{T_{s\ min}} + \frac{2.0\ \alpha\ \phi}{T_{v\ min} + T_{s\ min}} P \left\{ \frac{T_{v\ min} + T_{s\ min}}{2} \right\} \right.}{R \frac{n}{V_R}} \quad (2\text{-}28)$$

This equation defines the minimum reservoir volume for the case in which all the gas is located in the condenser and adiabatic sections. As the reservoir volume increases above the minimum, the minimum controller set point will increase until it reaches the value defined for an infinite reservoir. This condition is defined by the solution of the following equations.

$$P \left\{T_{v\ max}\right\} = P \left\{T_{R\ min}\right\} + \frac{n}{V_R} R\ T_{R\ min} \quad (2\text{-}29)$$

$$T_{v\ max} = T_{cs\ min} + \delta - \dot{Q}_{max} \left[\frac{1}{K_{ce}} + \frac{1}{K_{ev}}\right] \quad (2\text{-}30)$$

A similar development can be used to define the maximum controller set point temperature as defined by equations 2-22, 2-23, and 2-24. For an infinite reservoir volume, the maximum controller set point temperature is defined by the following equations.

$$P \left\{T_{v\ min}\right\} = P \left\{T_{R\ max}\right\} + \frac{n}{V_R} R\ T_{R\ max} \quad (2\text{-}31)$$

$$T_{v\ min} = T_{c\ max} - \delta - \dot{Q}_{min} \left[\frac{1}{K_{ce}} + \frac{1}{K_{ev}}\right] \quad (2\text{-}32)$$

For increasing set point temperature, compression of the non-condensible gas must occur since the pressure at the minimum vapor temperature continues to increase while the partial vapor pressure and the partial gas pressure in the reservoir remains constant.

The maximum controller set point temperature decreases with reservoir volume as shown by equations 2-22, 2-23, and 2-24. This continues until the

reservoir volume reaches the minimum for the maximum reservoir temperature corresponding to a controller set point temperature of

$$T_{cs\ max} = T_{R\ max} + \delta + \dot{Q}_{min} \left[\frac{1}{K_{ce}} + \frac{1}{K_{ev}} \right] \qquad (2\text{-}33)$$

This corresponds to a condition where the maximum reservoir temperature equals the minimum vapor temperature at the maximum controller set point temperature.

2.3 VCHP PSEUDO-TRANSIENT CONTROL ANALYSIS

The pseudo-transient model integrates the steady state control model with a reservoir transient response model, and calculates the minimum and maximum reservoir temperatures based on control and response requirements. For low capacitance control points, this analytical approach becomes and important consideration in preventing control point temperature excursions outside the temperature tolerance band. This approach shows that tremendous increases in required reservoir volume are necessary for rapidly responsing systems.

The reservoir transient response model uses a linearized conductance technique to simulate the transient radiation response. Figure 2-3 compares the response of the real reservoir with the response using the linearized technique, and shows that the linearized response is dependent on the end point temperature.

Simultaneously, the steady state control analysis, based on the calculated minimum and maximum reservoir temperatures, determines the required reservoir volume. This volume is then used for the next solution cycle. This process continues until the desired error is obtained.

In order to simplify the solution technique, the reservoir radiation conductance was linearized. For a given reservoir and sink temperature, the reservoir radiation conductance is defined as

$$K_T = \eta_R\ \sigma\ \varepsilon\ A_R \left\{ T_R^3 + T_s\ T_R^2 + T_R + T_s^3 \right\} \qquad (2\text{-}34)$$

The linearized conductance is defined as the integrated average of the

reservoir conductance from the minimum reservoir temperature to the maximum reservoir temperature. This results in the following equation.

$$K_L = \eta_R \varepsilon \sigma A_R \left[\frac{1}{4} \left\{ T_{R\,max}^{\,3} + T_{R\,min}\, T_{R\,max}^{\,2} + T_{R\,max}\, T_{R\,min}^{\,2} + T_{R\,min}^{\,3} \right\} + \right. \tag{2-35}$$

$$\left. \frac{T_s}{3} \left\{ T_{R\,max}^{\,2} + T_{R\,min}\, T_{R\,max} + T_{R\,min}^{\,2} \right\} + \frac{T_s^{\,2}}{2} \left\{ T_{R\,max} + T_{R\,min} \right\} + T_s^{\,3} \right]$$

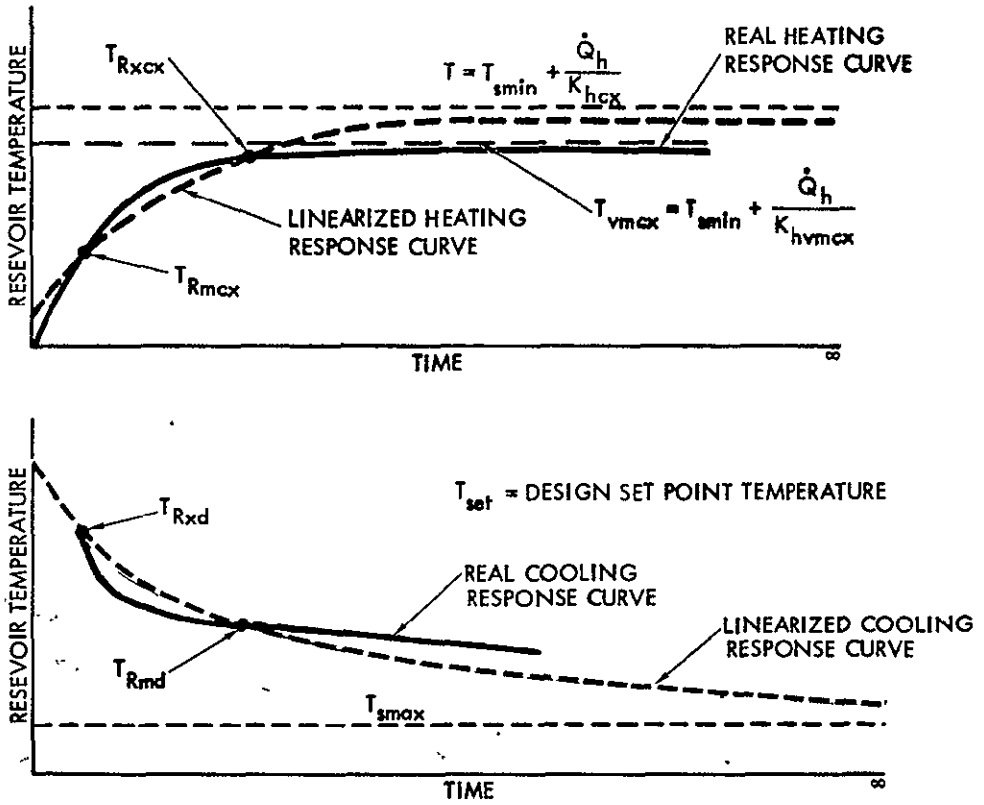

Figure 2-3 Real and Linearized Thermal Response Curves

The linearized conductance can now be used in a simple conduction network. Figure 2-4 shows such a network from which the following transient response equations were derived. The general equation for cooling response is,

$$T_R = \left(T_{R\ max} - T_s\right) \exp\left(-\frac{K_c}{C}\theta\right) + T_s \qquad (2\text{-}36)$$

The general equation for heating response is,

$$T_R = \left(T_{R\ min} - T_s - \frac{\dot{Q}_h}{K_h}\right) \exp\left(-\frac{K_h}{C}\theta\right) + T_s + \frac{\dot{Q}_h}{K_h} \qquad (2\text{-}37)$$

Pseudo-transient controllability of the FCHP requires that the reservoir be able to respond under worst case cooling and worst case heating conditions such that the control point temperature remains within the temperature tolerance band. Simultaneous solution of the heating and cooling response equations and the steady state control equations for a given design and specified maximum controller set point temperature is accomplished using iterative techniques.

The specified time response is based on the best case cooling response of the control point. Considerations that should be accounted for are environmental exposure time, time at minimum and maximum heat loads, thermal control system design, and the control point capacitance.

The worst case cooling and worst case heating conditions are defined as follows: The worst case cooling condition corresponds to natural radiation cooling at the design set point temperature. Worst case heating response occurs at the maximum specified controller set point temperature and is governed by the applied reservoir heater power. It is generally desirable that the worst case heating response be matched to the worst case cooling response. To define a minimum reservoir heater power, matching requires that the reservoir heater provide for worst case heating the same potential as the maximum sink temperature provides for worst case cooling. Since the worst case heating response occurs at the specified maximum controller set

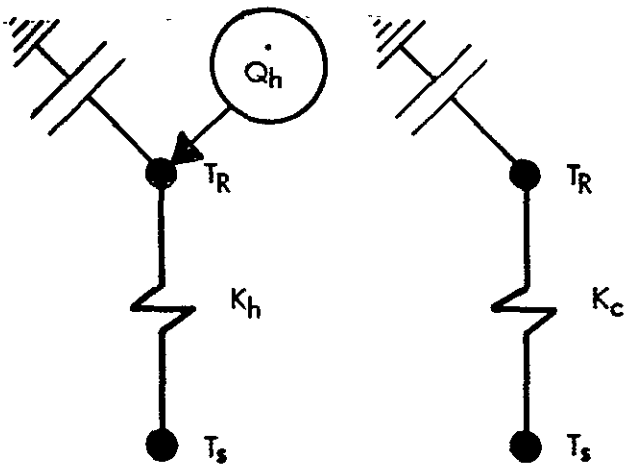

Figure 2-4 Reservoir Thermal Networks for Heating and Cooling

point temperature, the corresponding minimum vapor temperature should be the upper limit for reservoir temperature, such response corresponding to the constant application of maximum heater power. Therefore, the maximum reservoir heater power is defined as

$$\dot{Q}_h = K_{hvmcx} \left(T_{rmcx} - T_{s\ min} \right) \tag{2-38}$$

where

$$K_{hrmcx} = f \left(T_{Rmcx}, T_{vmcx}, T_{s\ min} \right) \tag{2-39}$$

The end point temperatures in the calculation of the linearized conductance are the minimum reservoir and minimum vapor temperatures, since the response calculations based on linearized conductances are valid only for the end points. Figure 2-3 shows that if K_{hcx} were used in place of K_{hvmcx}, then the upper limits of the reservoir temperature and the heater power would be low.

Since equation 2-39 is indirectly dependent upon T_{Rmcx}, it must be solved simultaneously with the following basic equations.

$$T_{Rmd} = \left(T_{Rxd} - T_{smax}\right)\exp -\left(\frac{K_{cd}}{C}\,\theta_1\right) + T_{smax}. \tag{2-40}$$

$$T_{Rmcx} = \left(T_{Rxcx} - T_{smax}\right)\exp -\left(\frac{K_{ccx}}{C}\,\theta_2\right) + T_{smax} \tag{2-41}$$

$$T_{Rxcx} = \left(T_{Rmcx} - T_{smin} - \frac{Q_h}{K_{hcx}}\right)\exp\left(-\frac{K_{hcx}}{C}\,\theta_1\right) + T_{smin} + \frac{Q_h}{K_{hcx}} \tag{2-42}$$

$$\left(T_{Rxd} = T_{rmd} - T_{smin} - \frac{Q_h}{K_{hd}}\right)\exp\left(-\frac{K_{hd}}{C}\,\theta_2\right) + T_{smin} + \frac{Q_h}{K_{hd}} \tag{2-43}$$

$$K_{cd} = f\left(T_{Rmd},\ T_{Rxd},\ T_{smax},\ A_{Res}\right) \tag{2-44}$$

$$K_{ccx} = f\left(T_{Rmcx},\ T_{Rxcx},\ T_{smin},\ A_{Res}\right) \tag{2-45}$$

$$K_{hd} = f\left(T_{Rmd},\ T_{Rxd},\ T_{smin},\ A_{Res}\right) \tag{2-46}$$

$$K_{hcx} = f\left(T_{Rmcx},\ T_{Rxcx},\ T_{smin},\ A_{Res}\right) \tag{2-47}$$

$$K_{hvmcx} = f\left(T_{Rmcx},\ T_{vmcx},\ T_{smin},\ A_{Res}\right) \tag{2-48}$$

$$\dot{Q}_h = K_{hvmcx}\left(T_{vmcx} - T_{smin}\right) \tag{2-49}$$

$$T_{vxd} = f\left(\dot{Q}_{hd}\right) \tag{2-50}$$

$$\left.\frac{n}{V_R}\right|_{ds} = f\left(T_{vxd},\ T_{Rmd}\right) \tag{2-51}$$

$$T_{vmcx} = f\left(\dot{Q}_{mcx}\right) \tag{2-52}$$

$$L_{bcx} = f\left(\dot{Q}_{mcx},\ T_{smin},\ T_{vmcx}\right) \tag{2-53}$$

$$\left.\frac{n}{V_R}\right|_{cx} = f\left(\left.\frac{n}{V_R}\right|_{ds},\ \dot{Q}_{xcx},\ \alpha',\ \beta'\right) \tag{2-54}$$

$$T_{Rmcx} = f\left(\left.\frac{n}{V_R}\right|_{cx}\right) \tag{2-55}$$

$$\frac{V_R}{V_c} = f\left(T_{Rmcx},\ T_{vmcx},\ T_{s\ min}\right) \tag{2-56}$$

Solution of these equations was accomplished with the aid of a computer program using iterative techniques.

2.4 FLUID INVENTORY ANALYSIS

The liquid inventory in a heat pipe varies as a function of temperature, but the total mass of the fluid is constant. Therefore, the amount of liquid in the pipe at any temperature can be determined by knowing the density of the liquid and vapor and the initial charge.

The initial charge is determined by,

$$m_i = \rho_\ell\ V_\omega + \rho_v\ V_{vs} \tag{2-57}$$

The volume of the wick in a VCHP includes the porus volume of the screen in the reservoir, the porous volume in the feeder tube wick, and the volume of the grooves. The grooves were assumed to be completely filled (flat menicus) rather than the average fill (30° menicus recession) normally used. This provided a margin of safety against insufficient fluid inventory.

The fluid charge required for the final design was calculated at 27.7 gm of ammonia, and with a 10% overfill the charge was 30.5 gm. The charge was calculated for an operating temperature of 30°C, which is the temperature with the greatest fluid inventory requirement. The actual pipe charge was 29.7 gm of ammonia, which is a 7% overcharge. Electronic grade ammonia with a purity of 99.9995% was used to minimize any degradation of performance due to impurities.

For a given charge and total volume, the following relationship defines the saturated liquid volume.

$$V_\ell = \frac{m_i}{(\rho_\ell - \rho_v)} - \frac{V_\omega + V_{vs}}{\left(\frac{\rho_\ell}{\rho_v} - 1\right)} \qquad (2\text{-}58)$$

The liquid excess is then defined as

$$\Delta V_{ex} = V_\ell - V_\omega \qquad (2\text{-}59)$$

Figure 2-5, which shows the amount of excess liquid in the vapor space as a function of temperature, this indicates that a pipe charged at 0°C will have a liquid volume of 3.00 cm^3 less than that required at 30°C. This would result in an estimated 40% degradation of the heat transport capability at 30°C. For a pipe charged at 30°C, there is sufficient liquid to obtain maximum heat transport capability from 0°C to 30°C. When gas is placed in the pipe and the reservoir is maintained at a lower temperature than the rest of the pipe, a slightly larger fluid charge is required. This effect is negligible in the present VCHP since the liquid inventory in the gas reservoir is relatively small (20% of total liquid) and the reservoir temperature is always within 13°C of the vapor temperature. This shows that a pipe filled to meet the fluid inventory requirements at 30°C will be capable of maximum heat pipe performance from 0°C to 30°C.

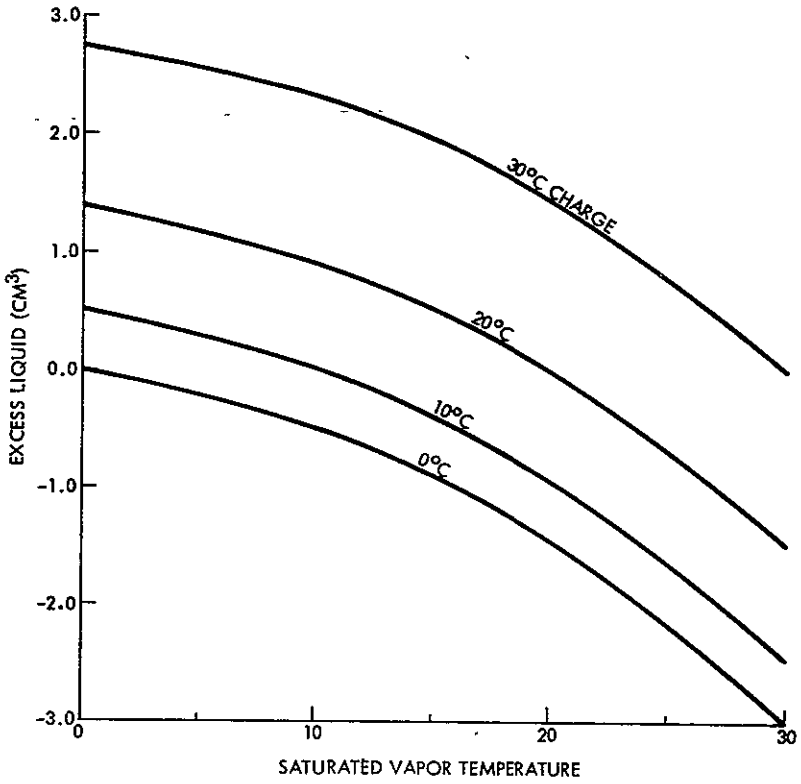

Figure 2-5 Excess Liquid in VCHP

2.5 NON-CONDENSIBLE GAS SELECTION AND INVENTORY

Gas selection was based on obtaining the lowest diffusion rate in the gas front region; therefore, a gas with a low diffusion coefficient in ammonia was desirable. Since experimental data is scarce, a Lennard-Jones potential technique was used to estimate the diffusion coefficients as a function of temperature (Reference 8). The Lennard-Jones equation for the diffusion coefficient with constituents A and B is

$$D_{AB} = \frac{.001858\ T^{\frac{3}{2}} \left[\frac{1}{M_A} + \frac{1}{M_B}\right]^{\frac{1}{2}}}{P\ \sigma^2_{AB}\ \Omega} \qquad (2\text{-}60)$$

where

T is the temperature in kelvins

M is the molecular weight

P is the pressure in atmospheres

σ is the collision diameter in Angstroms

and Ω is the collision integral.

The collision integral has been tabulated as a function of $T/k\varepsilon$ (References 8 and 18), where k is the Boltzman constant in ergs/K and ε is the energy of molecular interaction in ergs. Since ammonia is a polar molecule, adjustments must be made to σ and ε as described by Hirschfelder et. al. (Reference 8).

Figure 2-6 shows the calculated results for the binary diffusion coefficient for helium, neon, argon, and nitrogen gas in ammonia. These results were used cautiously, since analytical techniques to predict physical properties only approximate physical behavior. These results show that argon and nitrogen have the lowest diffusion coefficients. The difference between argon and nitrogen is insignificant for practical purposes. Solubility has also been used as a criteria for gas selection, but is generally important only when composite or arterial wicks are used. The solubility of argon in ammonia was estimated from data published by Hildebrand, et. al. (Reference 7). The rough estimate showed that less than .1% of the gas would be dissolved, producing a negligible effect on control of the VCHP.

The degradation in grooved heat pipe transport capability due to presence of non-condensible gas is on the order of 15% to 20%. Since the maximum heat load in this application was about 25% of the maximum transport capability, this degradation has no limiting effect. Finally, argon was selected for these tests based on its low diffusion coefficient. Experimental data only can provide the practical data necessary for gas selection between such close candidates as argon and nitrogen. The gas inventory, determined for the reservoir completely full at -12°C and the control point at 1°C, was 1.41 grams of argon. Argon with a purity of 99.995% was used to minimize performance degradation due to the presence of impurities.

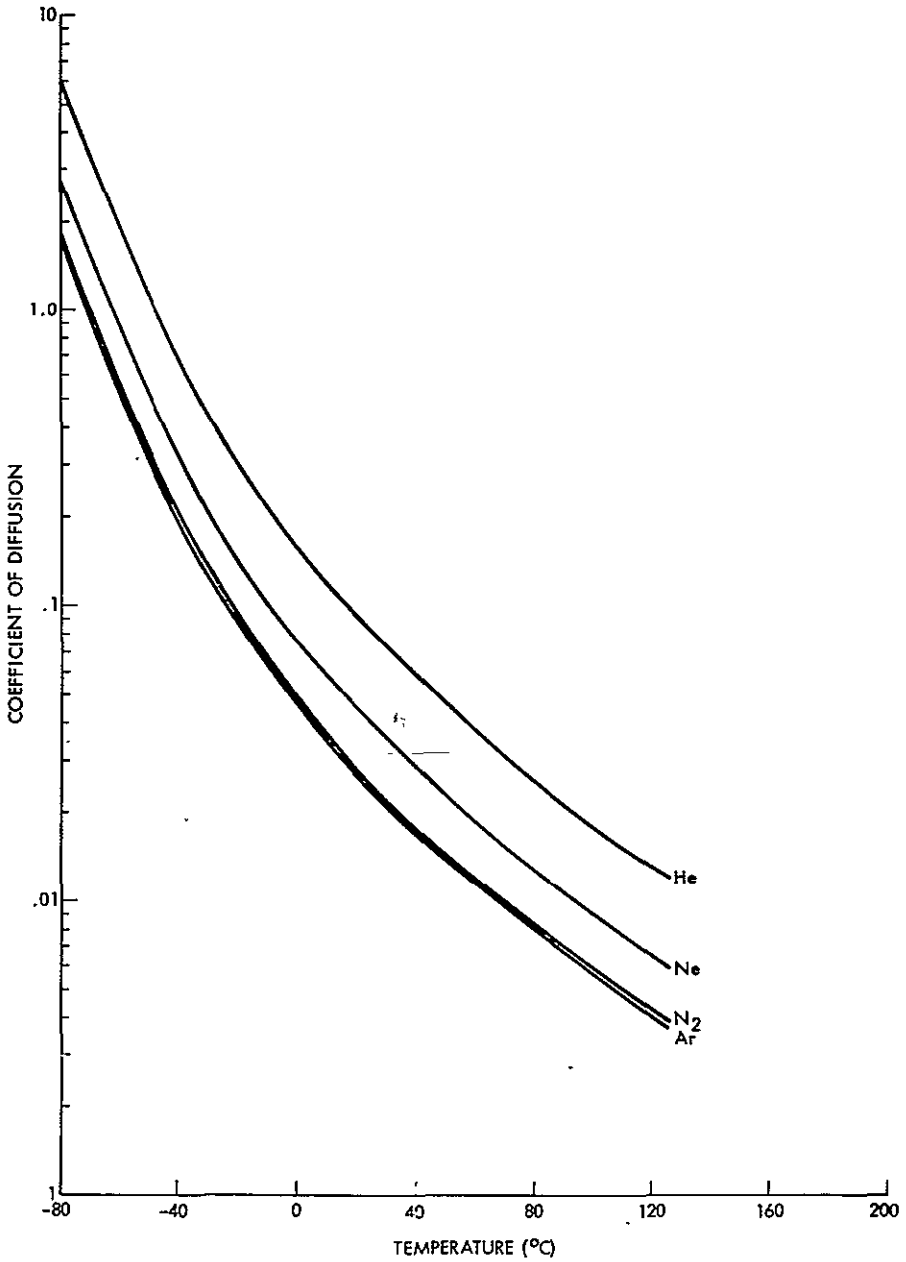

Figure 2-6 Gas Diffusion Coefficients

3.0 VCHP CONTROL PARAMETRICS

Both the steady state and pseudo-transient control analyses were based on maintaining control with the blockage length varying from zero to full condenser-adiabatic section blockage. For a blockage length of zero, the FCHP system heat rejection capability is a function of controller set point temperature as shown in Figure 3-1. Similarly, for full condenser-adiabatic section blockage the minimum heat load is found as a function of controller set point temperature. Figure 3-2 shows the required blockage length as a function of minimum rejected heat load for worst case cold condition. The discontinuity in the curve is due to the change in the analytical techniques used to determine the condenser and adiabatic blockage lengths. The minimum heat load variations applicable in the following pages are found on Figure 3-2 for the condition $\alpha = 1$. Temperature control of the FCHP system was specified to be within $\pm$ 1.0°C of the set point temperature. The radiator and the reservoir were exposed to a minimum environmental sink temperature of -120°C and a maximum environmental sink temperature of -13°C.

Steady state reservoir volume requirements are dependent upon the design set point temperature, the controller set point temperature, and restraints placed on the maximum reservoir temperature. Minimum and maximum effective sink temperatures also affect the volume requirements, but have been held constant in these analyses.

A map of reservoir volume requirements is shown in Figure 3-3. For the case of maximum reservoir temperature excursion (i.e., from T_{smax} to T_{vmin}). This figure also shows that increases in design set point temperature result in decreases in the reservoir volume requirements, while increases in controller set point temperature result in increases in reservoir volume requirements.

If the maximum and minimum reservoir temperature is restrained, very large increases in reservoir volume result for both design and controller set point temperatures. Figure 3-4 show reservoir requirements as a function of the design set point temperature and maximum reservoir temperature. These

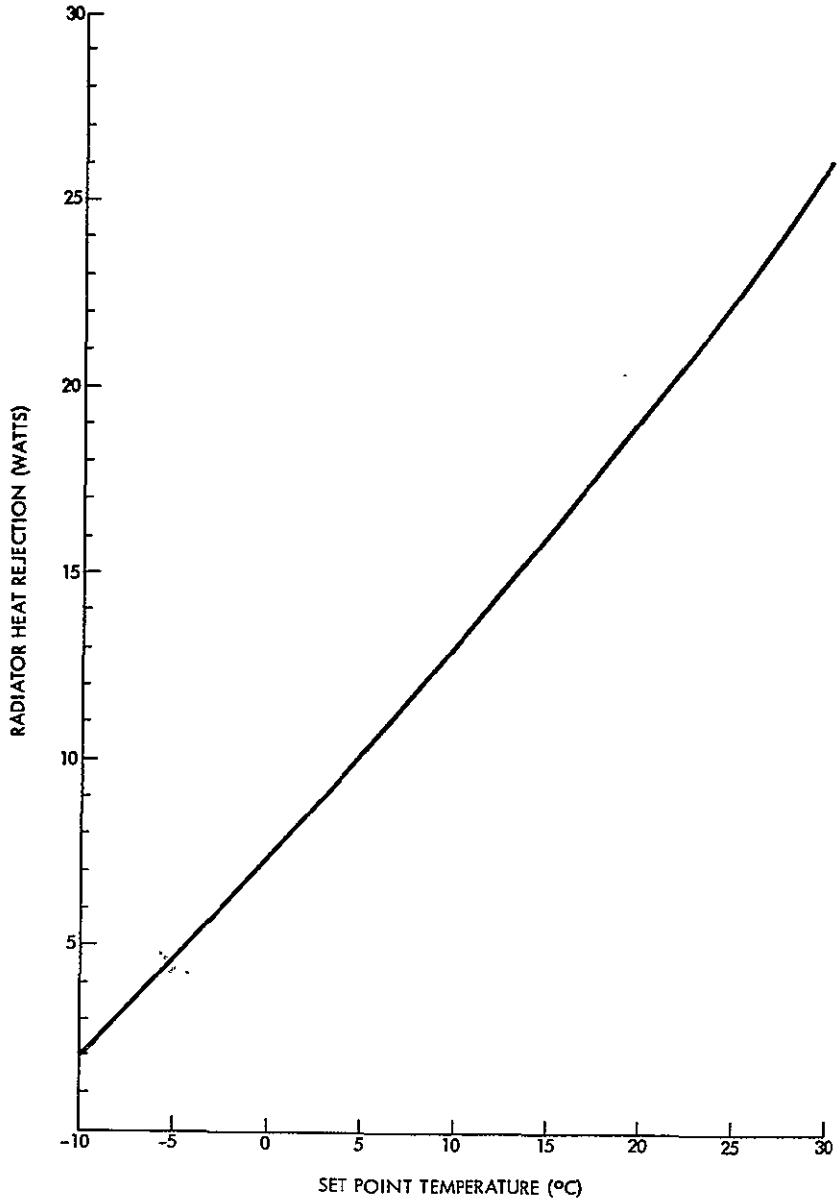

Figure 3-1 FCHP System Heat Rejection

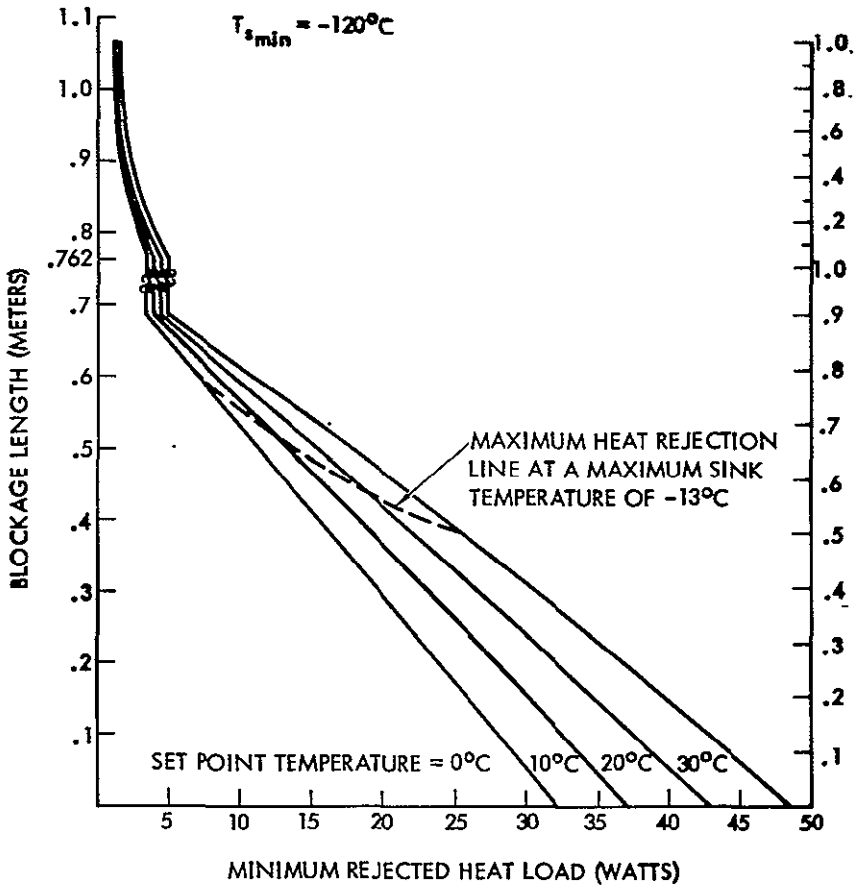

Figure 3-2 FCHP Required Blockage Length

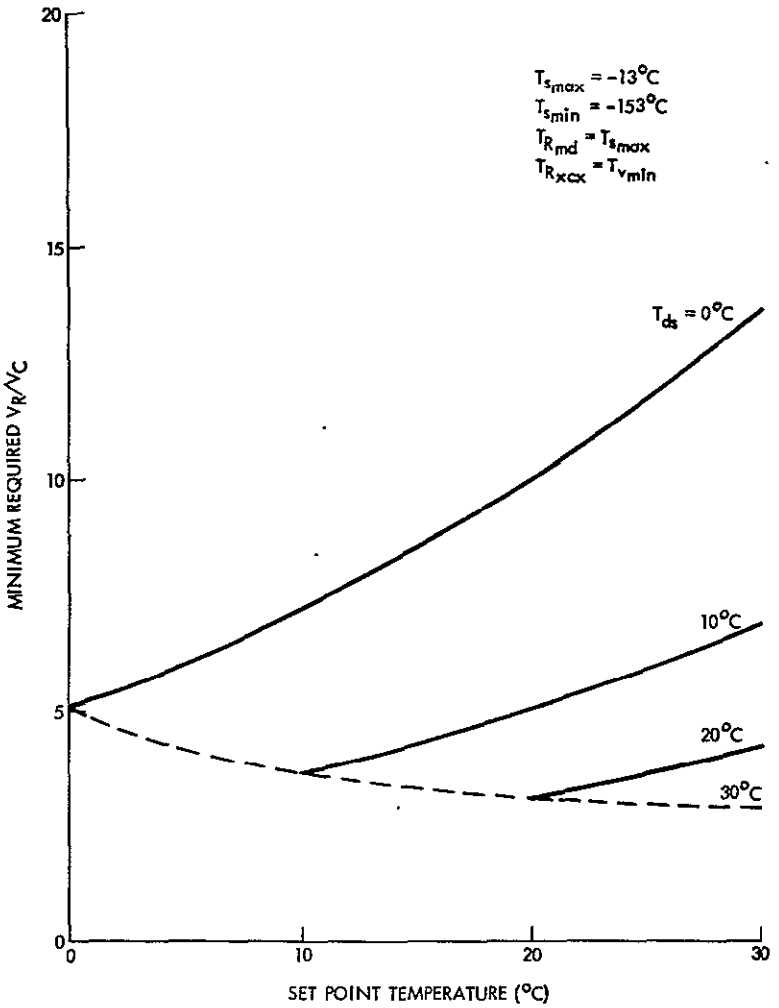

Figure 3-3 Required Reservoir Volume for $T_{Rmin} = T_{smax}$ and $T_{Rmax} = T_{vmin}$

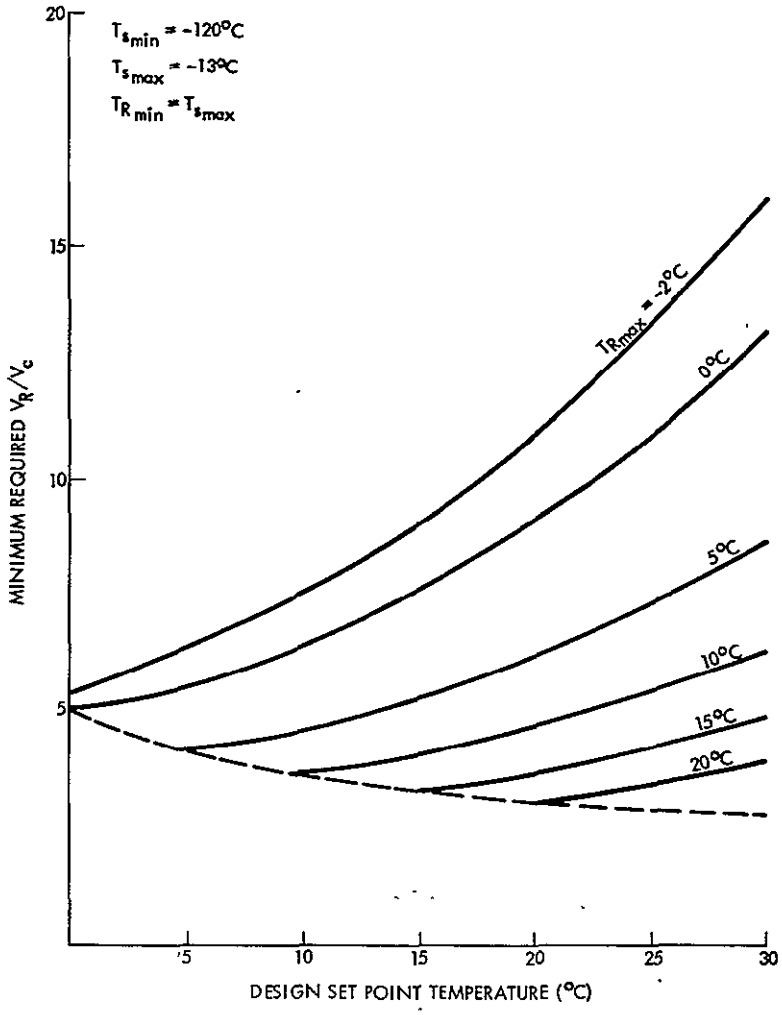

Figure 3-4 Required Reservoir Volume for Design Set Point Temperatures with Restrained Reservoir Temperature

requirements are not as severe as those imposed for the controller set point temperatures as shown in Figure 3-5. The explanation of these increases is that once the minimum vapor temperature reaches the specified maximum reservoir temperature, then control is maintained by increases in reservoir volume alone. This is clearly seen by the separation of the curves in Figures 3-4 and 3-5.

Figure 3-5 can also be used to determine the maximum controller set point temperature for a given reservoir volume. When this temperature is reached, all the gas in the FCHP is located in the condenser and adiabatic sections. Additional increases in reservoir temperature would theoretically result in compression of the gas front with no effect on set point temperature. In reality, however, an ustable condition would probably exist and vapor temperature oscillation would be expected. Figure 3-5 also shows that the design set point temperature affects the maximum controller set point temperature range. As the design set point temperature is raised, the controller set point temperature range becomes smaller.

At the top of Figure 3-5, the maximum controller set point temperature is indicated for an infinite reservoir. This is the point at which the sum of the partial gas pressure and partial vapor pressure in the reservoir equals the vapor pressure at the minimum vapor temperature. Control is not possible beyond this point because of compression of the non-condensible gas.

The reservoir volume requirement for a FCHP system requiring rapid response may increase very significantly over steady state requirements, especially in the case of low capacitance control point systems, in which a rapid response time is necessary to keep the FCHP system within the control point temperature tolerance band.

For the pseudo-transient analysis, the reservoir volume increases with decreasing design set point temperature and with increasing controller set point temperature (Figures 3-6 and 3-7). These figures show that the specified response time increases, the reservoir volume requirements decreases; The limiting case is the steady state result.

The (minimum) reservoir heater power requirements are shown in Figures

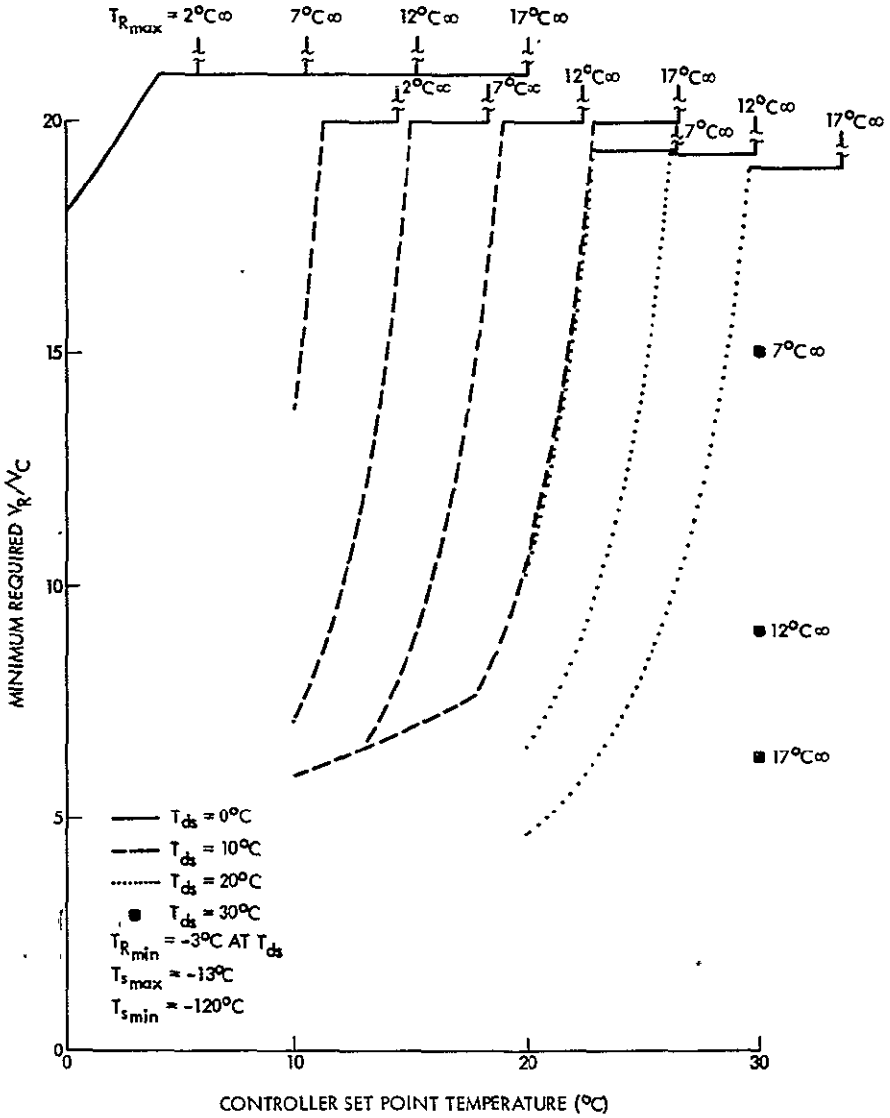

Figure 3-5 Required Reservoir Volume for Controller Set Point Temperatures with Restrained Reservoir Temperature

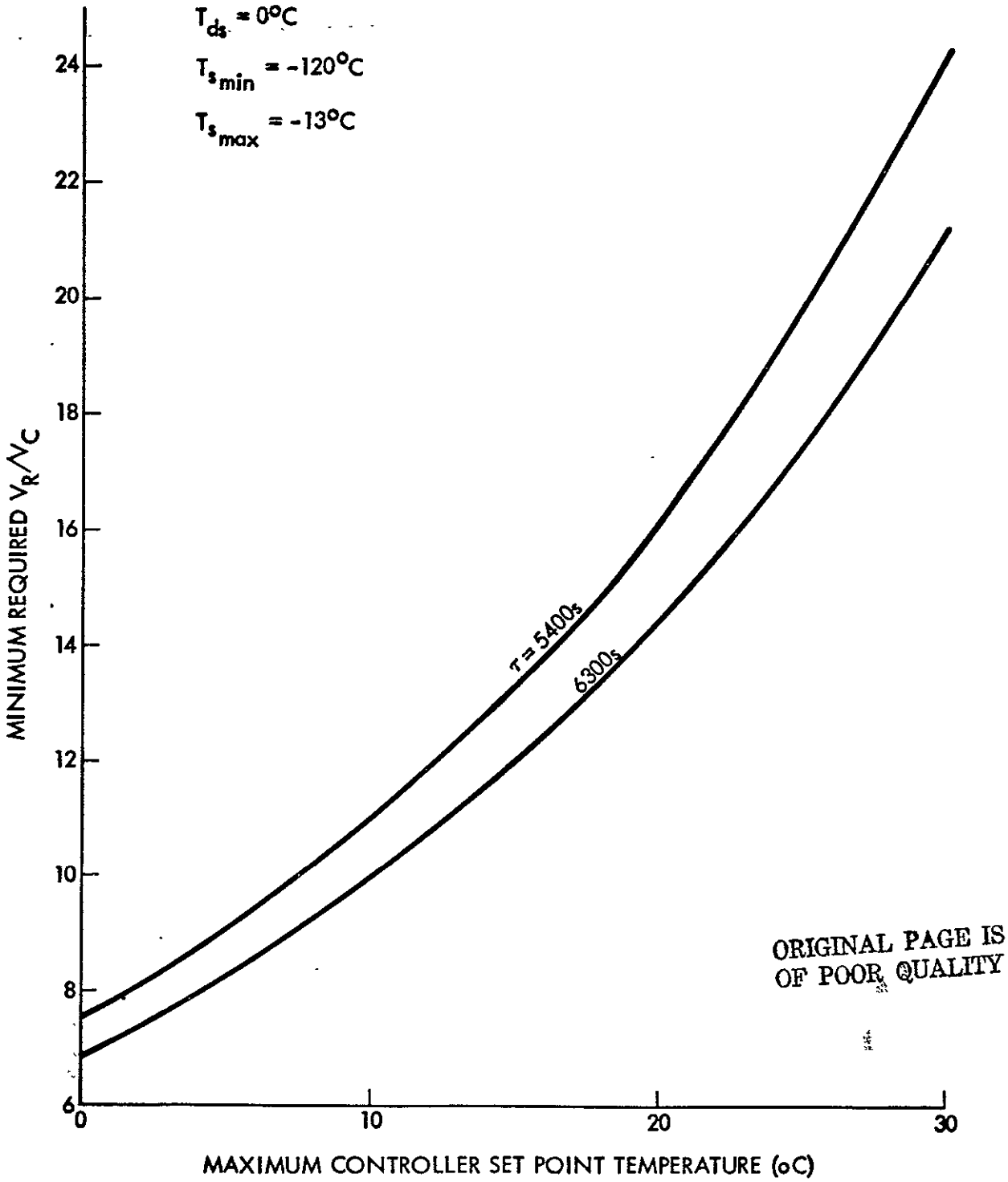

Figure 3-6 Required Reservoir Volume for Pseudo - Transient Analysis at T_{ds} = 0°C

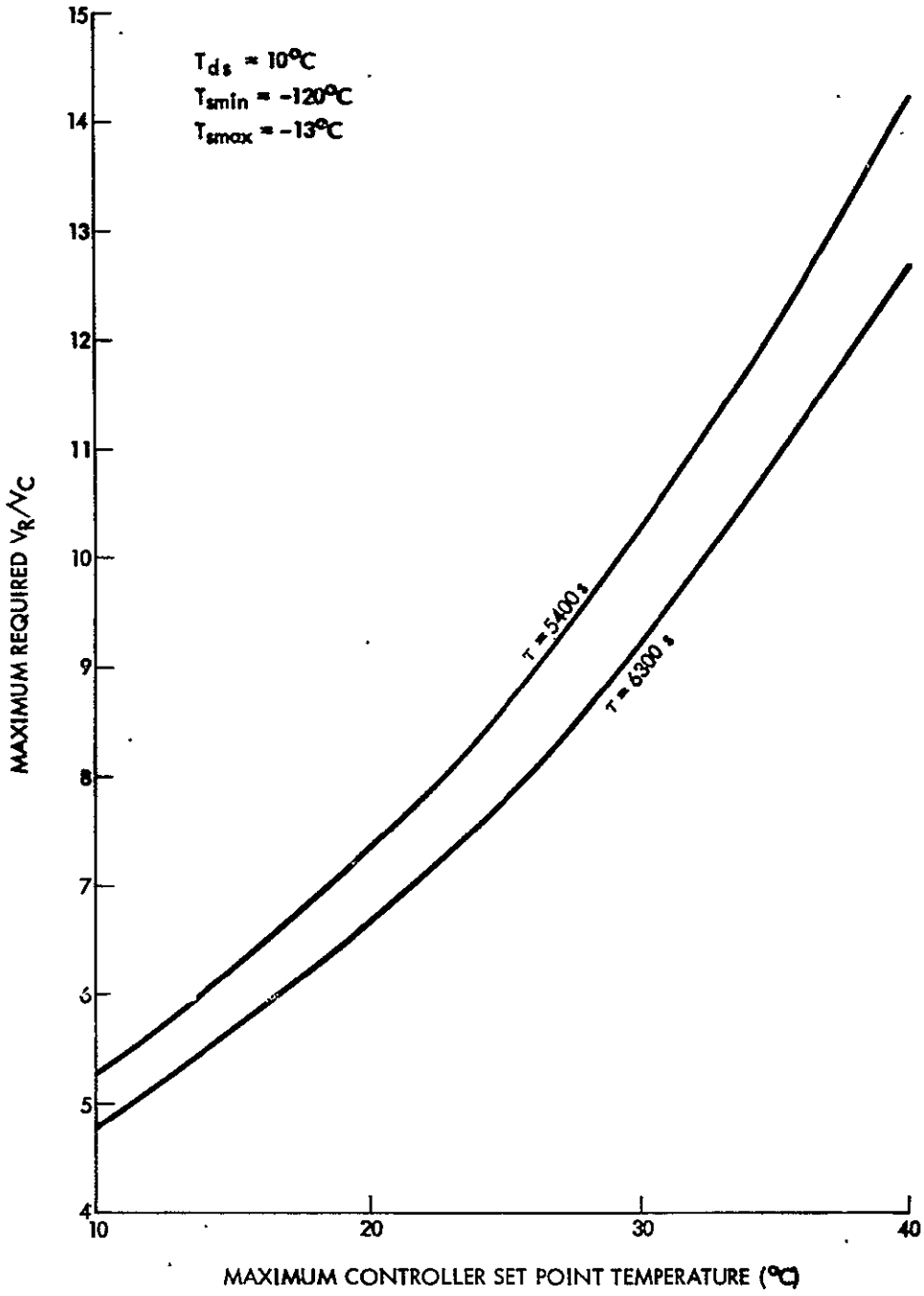

Figure 3-7 Required Reservoir Volume for Pseudo-Transient Analysis at T_{ds} = 10°C

3-8 and 3-9. In line with the reservoir volume requirements, the minimum reservoir power requirements increase with decreasing design set point temperature and with increasing controller set point temperatures. Also, the minimum heater power requirements decrease with increases in the allowed reservoir response time.

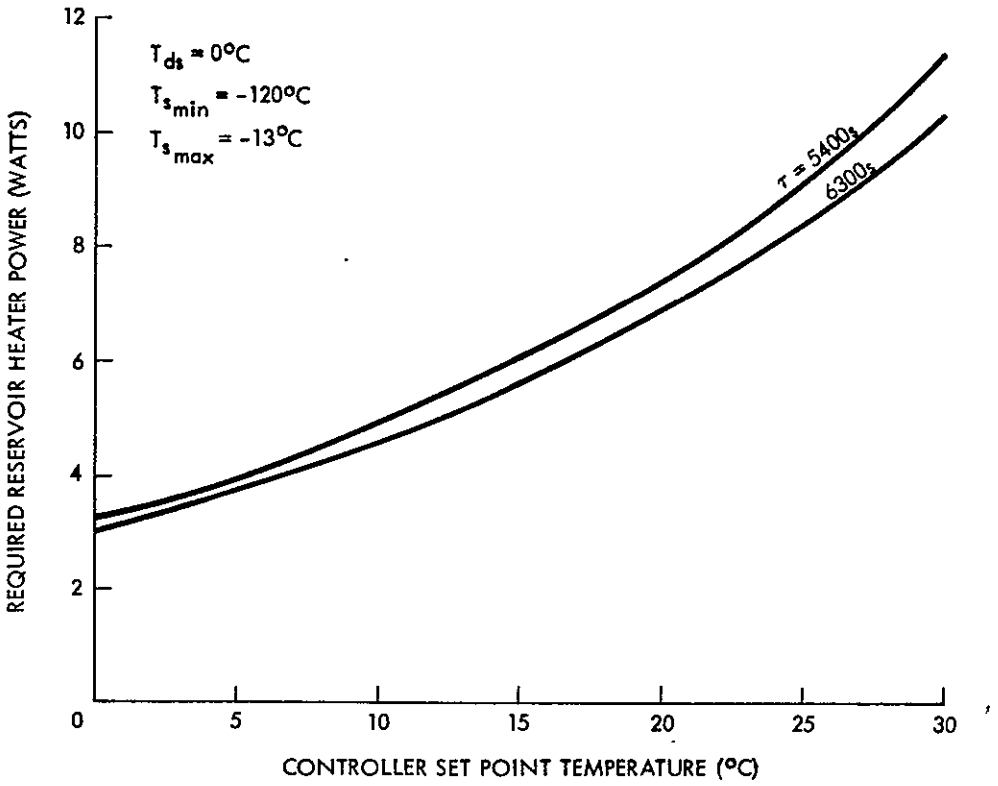

Figure 3-8 Minimum Power for Pseudo-Transient Analysis at T_{ds} = 0°C

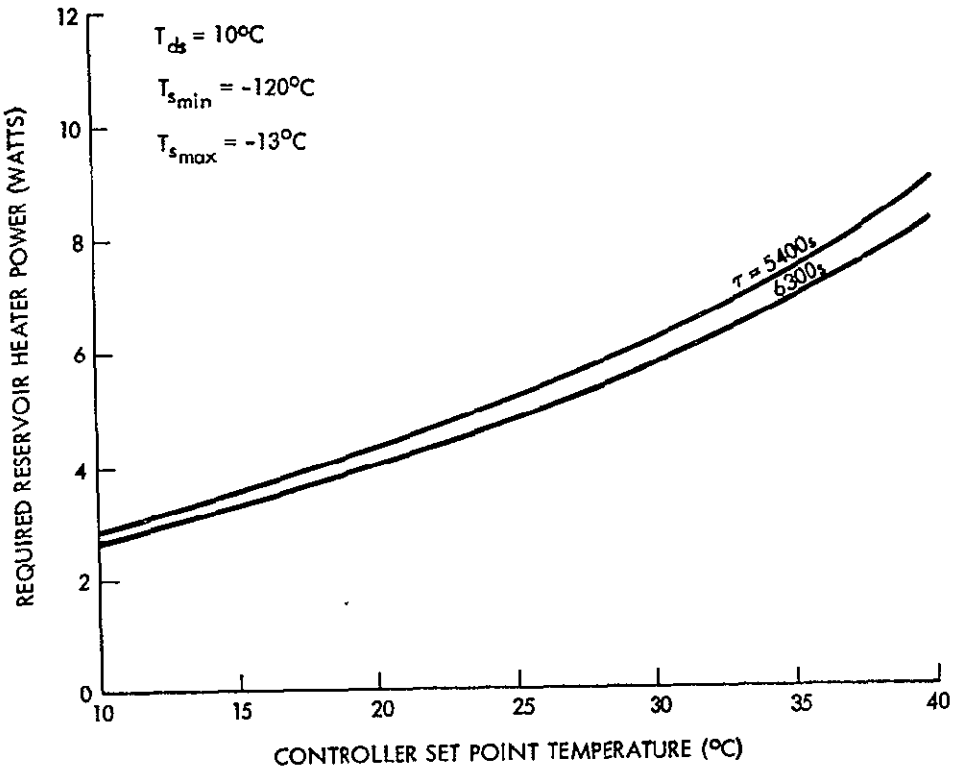

Figure 3-9 Minimum Power for Pseudo-Transient Analysis at T_{ds} = 10°C

4.0 DETAILED DESIGN, FABRICATION AND PROCESSING

The detailed design defined the final configuration for the VCHP. Considerations included in the design were performance, control, structural integrity, handling, and the resolution of potential problems. The final design was fabricated in accordance with Rockwell procedures for fabrication, assembly, and quality assurance of heat pipes. The completed pipe was finally baked out and charged with fluid and gas.

4.1 DETAILED DESIGN

The final design is shown in Figure 4-1. The heat transport section consists of an RM-20B grooved 6063-T6 aluminum heat pipe extrusion with a 38.1 cm (15 in) evaporator section, a 30.48 cm (12.0 in) adiabatic section, and a 76.2 cm (30 in) condenser section. A 5.0 cm (2.0 in) mounting flange is provided in the evaporator and condenser sections. The adiabatic section wall thickness is .072 cm (.029 in), which translates to a factor of safety for pressure containment of approximately 20 based on operating pressure of 200×10^4 N/m^2 (290 psi). On each end of the thin wall adiabatic sections are 1.27 cm tapers, which gradually reduce the wall thickness of the heat pipe extrusion to prevent high stress concentrations. The relatively thick wall prevents buckling and handling problems associated with extremely thin-wall sections. Another consideration is the minimum heat leak through the adiabatic section. Figure 3-2 shows a heat leak of about 1-2 watts for full adiabatic blockage. A slightly greater heat leak can be expected due to diffusion heat transfer through the gas front. Diffusion heat transfer in the adiabatic section should be greater than that observed in the condenser section because of the low gas concentrations. The upper limit of heat transfer for full adiabatic section blockage is estimated at about 3.7 watts, assuming that the radiation conductance to space is infinite.

The condenser section has mounting flanges 2.54 cm (1.0 in) in length and separated by 1.27 cm (.50 in) slots. In these slots, the wall thicknesses were reduced to a diameter of 1.22 cm (.480 in). This was done to reduce the conduction heat transfer through the heat pipe shell and provide a sharper

gas front and therefore better control characteristics.

The non-condensible gas reservoir is sized to provide a reservoir-to-condenser volume ratio of ten to one. The extensive control analysis performed after the 10:1 reservoir had been constructed indicated that a minimum reservoir-to-condenser volume ratio of 13.6 would give better control for the present requirements. Less severe heat load or environmental constraints imply smaller reservoir volume requirements. Another consideration in reservoir sizing is transient time response. If the reservoir heating and cooling rates are the dominant limiting factors determining system response, then larger reservoir sizes should be expected (see Figures 3-6 and 3-7). further test data and analyses are needed to clarify the role of reservoir transient response in relation to overall system transient response.

In order to produce a highly responsive reservoir, the thermal capacitance must be minimized. As a result, minimum wall thicknesses consistent with the safety considerations are desirable. Again the wall thickness of the reservoir was made thicker than necessary to prevent handling problems. The "hoop" stress safety factor for the reservoir is about 7.9. The ends of the reservoir were made from .318 cm (.125 in) 316 stainless steel plate sheet to reduce the stress concentration in the weld zone.

To isolate the reservoir thermally from the condenser section of the heat pipe, a 5.08 cm (2.0 in) long stainless steel feeder tube is used. This feeder tube is machined from an aluminum-stainless steel inertia-welded transition section, and has a wall thickness of .064 cm (.025 in) and a diameter of .795 cm (.313 in). The maximum heat leak through the feeder tube under the worst case conditions is less than .76 watts.

One layer of 200 mesh stainless steel screen is used to line the reservoir walls. A layer of 30 mesh screen is used to retain the 200 mesh screen in contact with the cylindrical wall of the reservoir. Three layers of screen line the bottom of the feeder tube and are held in contact with the three lower grooves of the condenser section by a cantilever spring. The three layers were used to provide liquid transport from the reservoir back to the condenser. In addition, the reservoir was elevated slightly by incorporating a slight bend in the feeder tube section. This prevents

transport degradation due to siphoning of liquid from the condenser section.

4.2 VCHP FABRICATION

The variable conductance heat pipe consists of three subsections - the heat pipe, the feeder tube transition, and the reservoir. The heat pipe, a 6063-T6 aluminum RM-20B extrusion, is machined to the configuration shown in Figure 4-1. It is comprised of the condenser, evaporator, and adiabatic sections. To attain this shape, the following sequential operations were performed:

- The extrusion was cut to length.
- The internal grooves, on both ends, were gas tungsten arc (GTA) welded with 4043 filler alloy to a depth of about 1/8 inch.
- The flange was milled off and then the various sections were turned as noted.
- Both ends were faced squared and the internal diameters were bored to 0.338 inch diameter.
- The lower three "teeth" were broached to remove 0.015 inches for a length of 1 inch.

The reservoir components are machined according to the specification on Figure 4-1. An aluminum-stainless inertially steel welded transition joint was obtained from the vendor and machined to the specification on the drawing.

Finally, the reservoir and feeder tube wicks are fabricated as shown in Figures 4-2, 4-3, and 4-4. All the wicks were made from 316 stainless steel screen. The reservoir primary wick and the feeder tube wick were cut from 200 mesh screen. The 30 mesh retainer screen was cut to hold the primary cylindrical wick against the reservoir wall. The finished VCHP components are shown in Figure 4-5. The fill tube aluminum extrusion and the feeder tube transition section were cleaned according to the following procedure:

- Immersed in hot trichloroethylene for 5 minutes.
- Flushed with Turco 49 (MB0210-008) at 74°C (165°F) for 10 munutes.

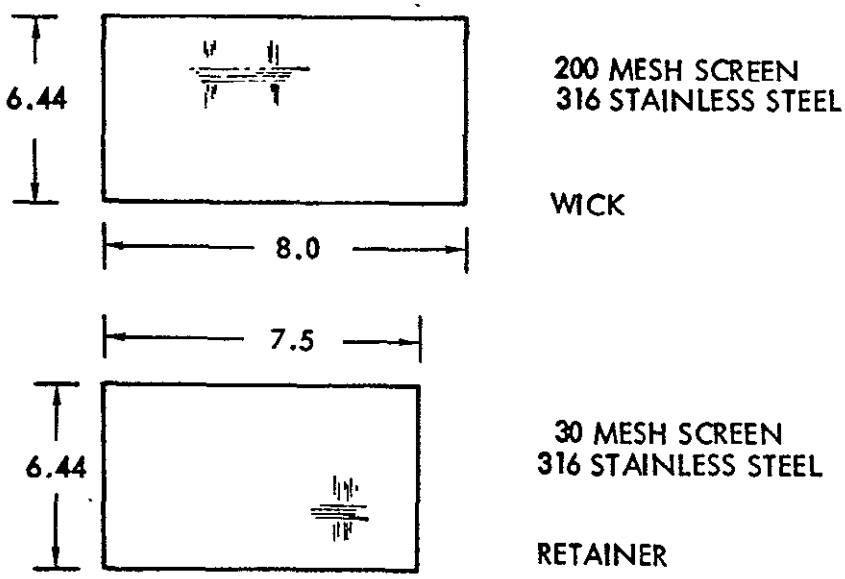

Figure 4-2 Primary Reservoir Wick and Retainer Screen

- Rinsed with tap-water followed by a DI water rinse.
- Flushed with 10% HNO_3 at room temperature.

The stainless steel reservoir components were cleaned according to the following procedure:

- Immersed in hot trichloroethylene for 5 minutes.
- Flushed with Turco 49 (MB0210-008) at 74°C for 10 minutes.
- Rinsed with tap-water followed by a DI water rinse.
- Flushed with 20% NHO_3 at 77°C (170°F).
- Rinsed with DI water - dried.

After cleaning, the VCHP components were assembled in the following manner:

Reservoir end cap wicks were resistance welded to the end caps.

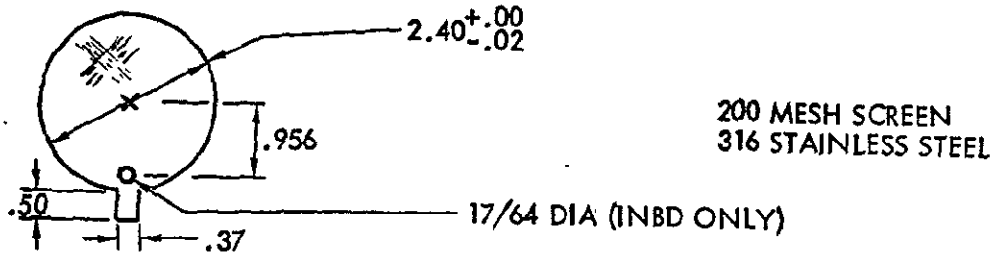

Figure 4-3 Reservoir End-Cap Wick

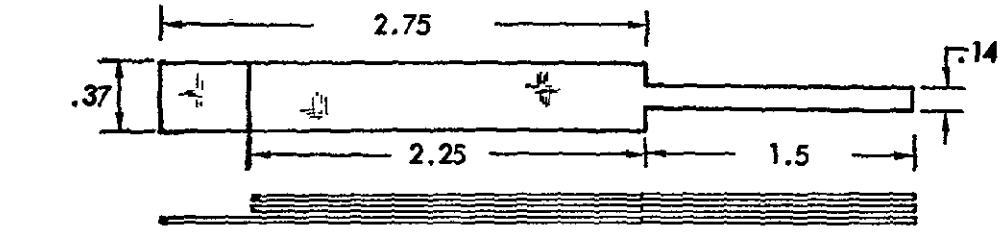

MATERIAL: 200 MESH SCREEN
316 STAINLESS STEEL

Figure 4-4 Feeder Tube Wick

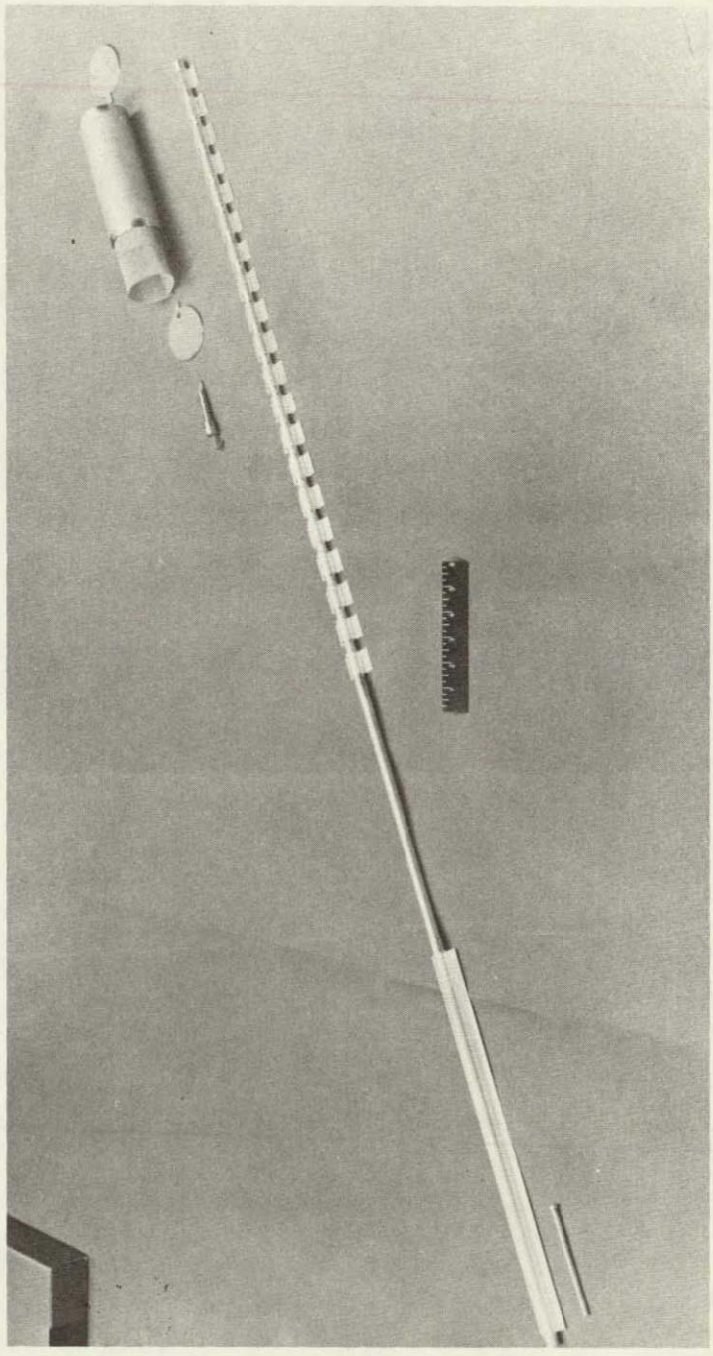

Figure 4-5 VCHP Components

- The stainless steel end of the feeder tube was gas tungsten arc (GTA) welded to the inboard end cap.
- The feeder tube wick was installed and formed tightly around the aluminum protrusion that would maintain the wick in the broached slot of the heat pipe condenser section. Figure 4-6 shows the wick and feeder tube carefully positioned in the broached slots, the aluminum end of the transition joint was GTA welded to the extrusion.
- The 200 mesh reservoir primary wick was positioned in the reservoir cylindrical section and was held in place by the 30 mesh retaining screen.
- The tab from the end cap wicks and the feeder tube wick were inserted under the retainer screen and the end caps GTA welded to the reservoir cylindrical section.
- Finally the fill tube was GTA welded to the evaporator end of the heat pipe. Figure 4-7 shows the completed VCHP.

For all stainless steel GTA welds, type 347 filler alloy was used; and for all aluminum GTA welds type 4043 filler alloy was used.

The completed unit was successfully proof pressure tested at 400 psig and Helium leak tested at 200 psig with no detectable leaks at a sensitivity of 3.9×10^{-10} SCCS on a CEC Helium leak detector.

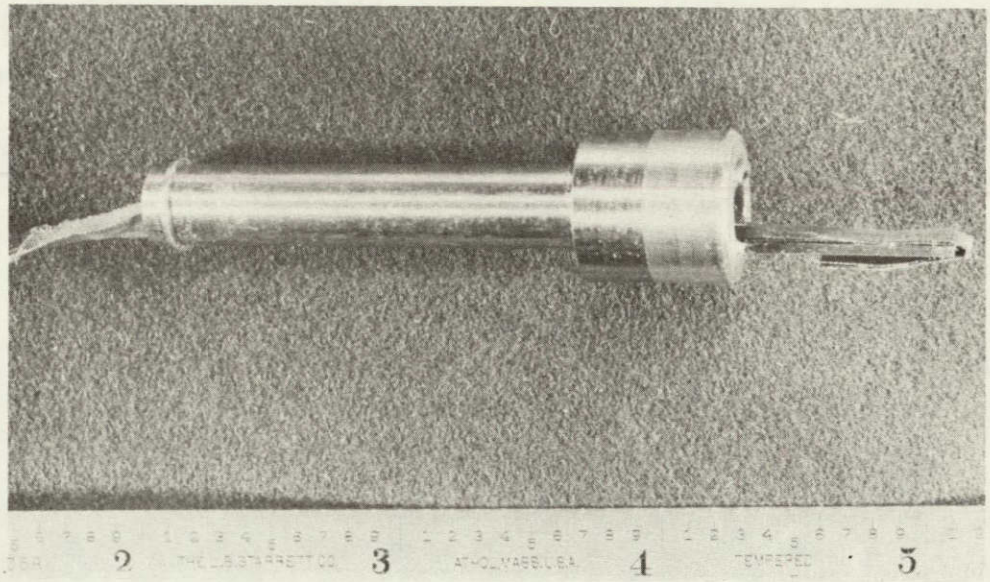

Figure 4-6 Transition Section and Feeder Tube Wick

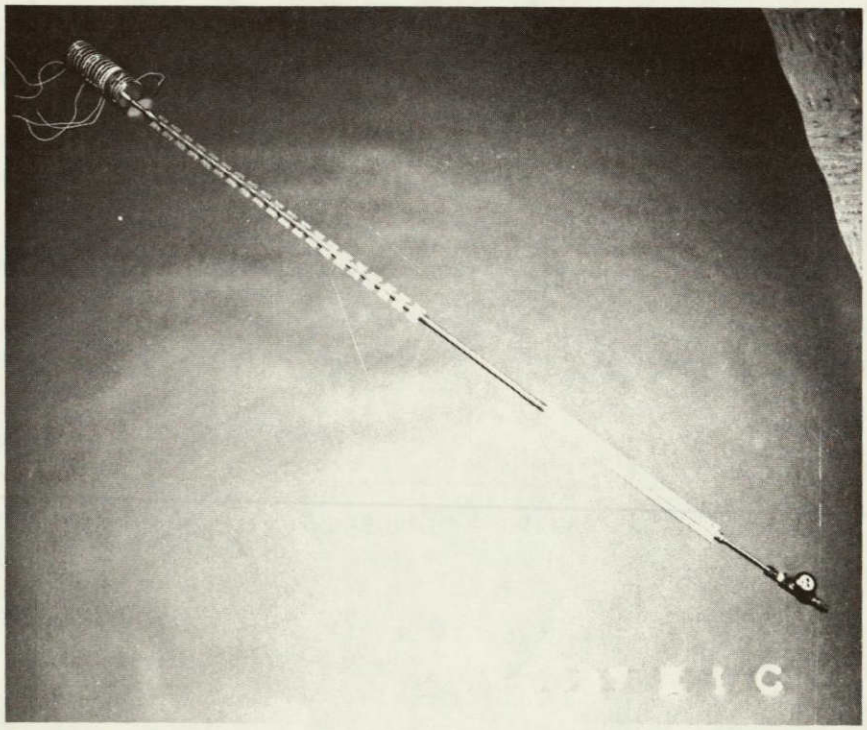

ORIGINAL PAGE IS
OF POOR QUALITY

Figure 4-7 Assembled VCHP

4.3 BAKEOUT

The completed pipe was degassed by bakeout under high vacuum before filling with working fluid and non-condensible gas. The following procedure was used for the bakeout process:

- Place the heat pipe in a bakeout oven and connect the vacuum-fill system.
- Open the fill valve and evacuate the pipe to a pressure of less than 10^{-6} torr.
- Bring the bakeout oven to a temperature of 115°C and maintain within $\pm$ 5°C for the duration of the bake.
- After a minimum of 16 hours close the fill valve and remove the pipe from the oven.

4.4 FLUID AND GAS CHARGING

The VCHP was filled with 29.7 gm of ammonia working fluid and 1.41 gm of argon gas. For the ammonia fill, a detailed working fluid fill procedure and check list was followed by the heat pipe laboratory personnel. The procedure followed was:

- Weigh the empty heat pipe.
- Insert the control volume containing the desired amount of working fluid into the fill apparatus as shown in Figure 4-8.
- Evacuate the fill system to a pressure of less than 5 millitorr.
- Isolate the vacuum system from the fill system.
- Fill the control volume with ammonia.
- Isolate the control volume from the ammonia supply cylinder.
- Transfer fluid by heating control volume to pro-

vide a pressure difference between the heat pipe and control volume.

- Close heat pipe valve.
- Weigh heat pipe to verify charge.

Similarly, a detailed non-condensible gas fill procedure and checklist was followed. The gas fill system is shown in Figure 4-9. The procedure followed was:

- Weigh the heat pipe
- Place the VCHP in LN_2 to freeze the working fluid, and open the heat pipe fill valve.
- Pressurize the control volume (v) to the initial pressure (P_i) and then isolate it from the argon cylinder.
- Knowing the initial pressure (P_i) and volume (v) of the control volume, calculate the final pressure (P_f) for a specified mass transfer (m_g) using the non-condensible gas charge equation of mass .

$$m_g = \frac{P_i - P_f \; V \; M.W.}{1205 \; T} \text{ (grams)}$$

where

P_i = initial manifold pressure (psia)

P_f = final manifold pressure (psia)

R = universal gas constant (1205 psia-cm^3/gm-K°)

V = control volume (cm^3) = 818 cm^3

T = charging gas temperature (°K)

M.W. = molecular weight (39.948 for argon)

- Meter transfer valve to reduce control volume pressure.
- Close heat pipe fill valve.
- Weigh the heat pipe to verify charge.

5.0 TEST AND RESULTS

A test program was undertaken with three prime objectives: determine the heat transport capability; determine the steady state performance; and determine the transient response characteristics. Following the test program, the results were correlated with theory and design and test recommendations defined.

The VCHP test fixture was built under the Space Division IR&D program. It consists of copper fins attached to an LN_2 reservoir, with a row of heaters bonded to the fin at the same distance from the heat pipe attachment point (Figure 5-1). The fixture is used to simulate the radiation heat sink.

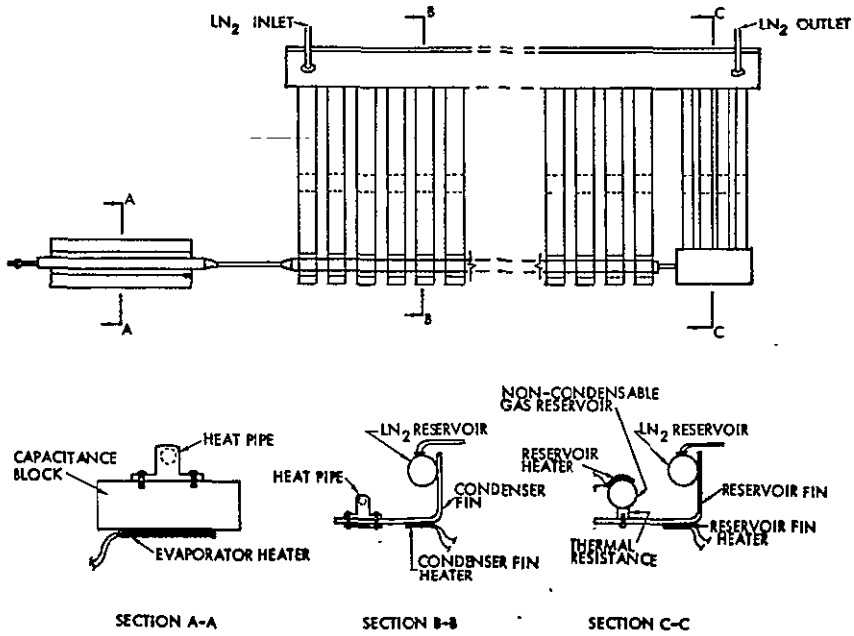

Figure 5-1 VCHP Test Fixtured

Application of heat to the heater changes the effective sink temperature by varying the temperature of the fin at the heater point. Figure 5-2 shows both theoretical curves and the experimental data points obtained for sink temperature with no load.

The heaters on the condenser fins were placed about 8.5 cm away from the pipe. This adequately simulates the -13°C sink temperature for both the blocked and unblocked parts of the condenser, but only simulates the blocked portion at -120°C. On the reservoir, a thermal resistance was used between the reservoir and reservoir fins. This resulted in adequate cooling response at the 0°C set point, but provided excessive cooling response for the 30°C set point.

In the heat transport test, the pipe was insulated with fiberglass and bench tested. For the control and transient test, the pipe was insulated with MLI and tested in the vacuum chamber.

5.1 HEAT TRANSPORT TESTS

The heat transport capability of the pipe was tested before and after the addition of gas into the pipe. These were bench tests with the pipe temperature at 20°C. Figure 5-3 shows the results of these tests.

The maximum heat transport predicted was 128 watts at zero adverse tilt. At 0.5 cm (.20 in) tilt, 70 watts was calculated. The experimental values obtained for zero and 0.5 cm tilt were 160 watts and 70 watts respectively. Performance at zero tilt was significantly better than predicted. This result is attributed to a condenser puddle which probably existed at zero tilt. At the .5 cm tilt, the experimental data agreed with the performance.

Before adding gas to the VCHP, a test was made to show the effect of the reservoir condensation rate on the transport capability. Figure 5-4 shows the maximum heat transport as a function of reservoir sink voltage (reservoir fin heater voltage). As the reservoir sink voltage increases (which is equivalent to increasing the sink temperature) an increase in the maximum heat transport capability occurs. This indirectly checks the pumping capability of the feeder tube wick, since burnout is occuring because liquid is being trapped in the reservoir. This occurs because the condensation rate into the reservoir is greater than the transport rate out.

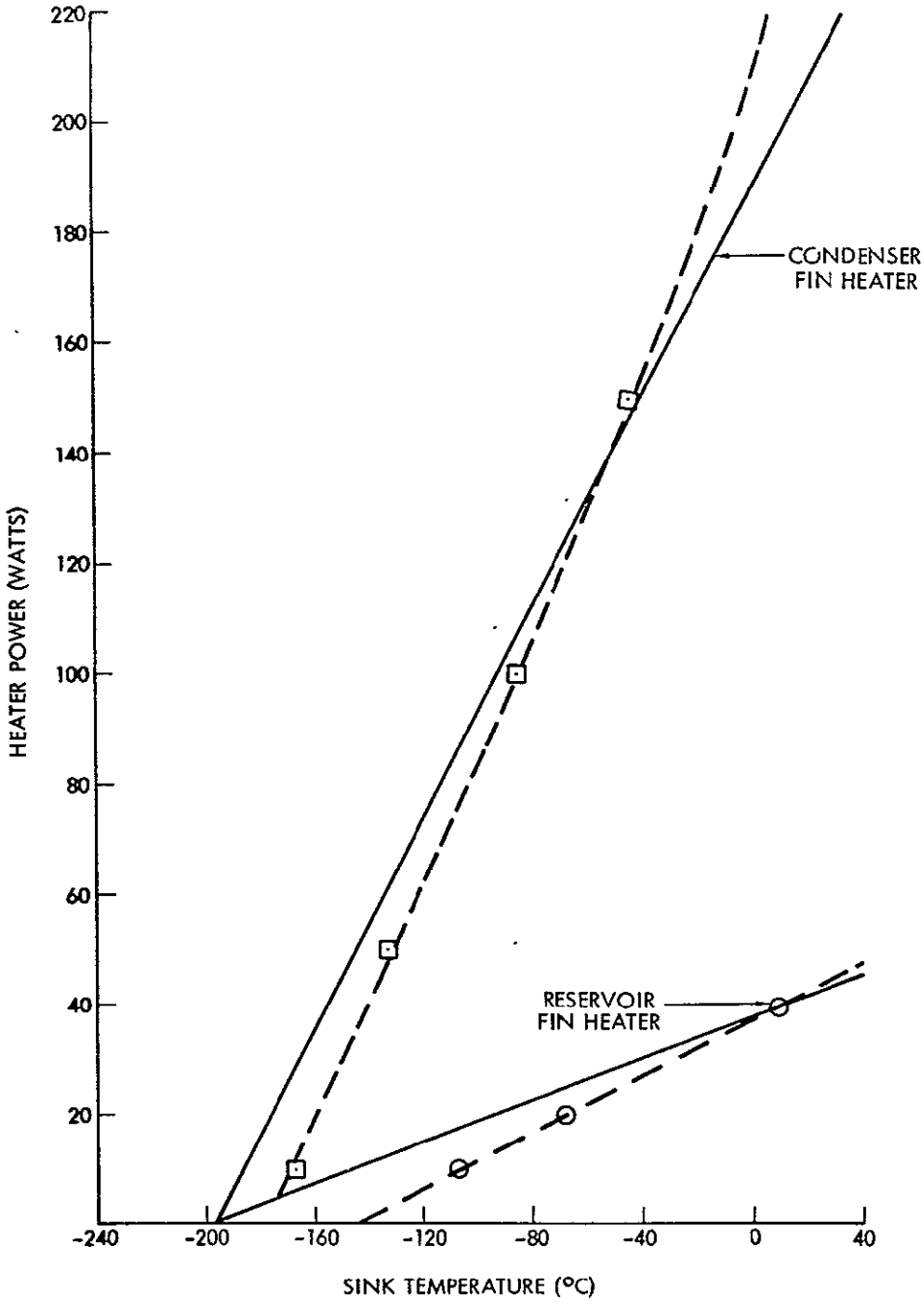

Figure 5-2 Theoretical and Experimental Heater Powers for Sink Temperature

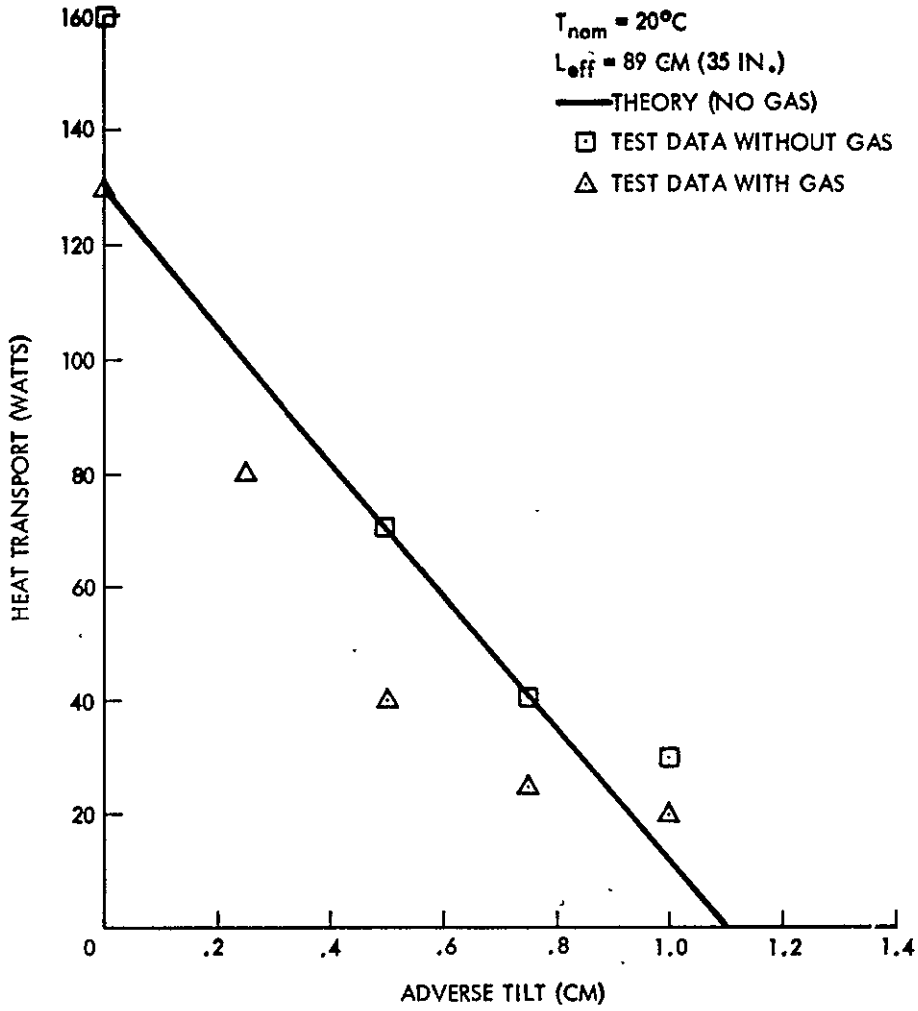

Figure 5-3 Theoretical and Experimental Heat Transport

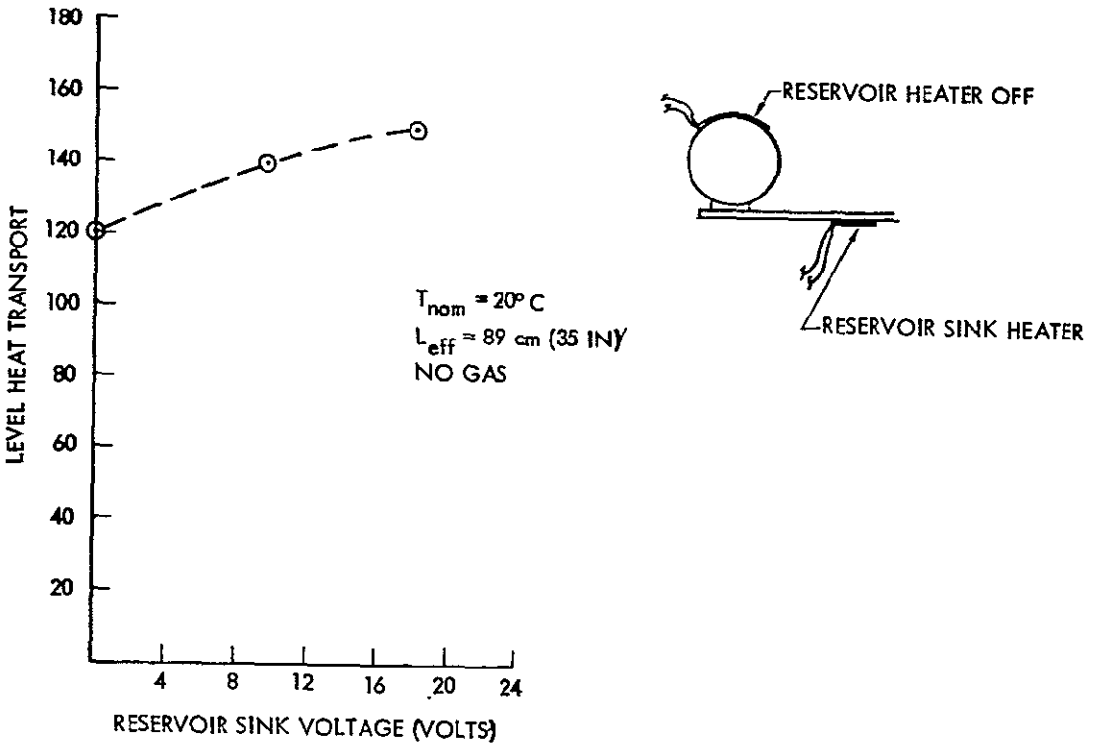

Figure 5-4 Heat Transport vs. Sink Voltage

When gas was added to the VCHP, the performance dropped off significantly. Heat transport dropped off about 18% at zero tilt, about 43% at 0.5 cm, and about 30% near the wick static height. This test data supports one hypothesis that degradation is due to non-condensible gas bubbles in the evaporator grooves. When at zero tilt, the length of the bubble is relatively short, and therefore there is only a small amount of performance degradation. As the tilt of the pipe is increased, the average liquid pressure surrounding the bubble decreases. This results in the bubble expanding accompanied by an additional degradation in performance. As the static height is approached, the puddle reduces the effective adverse tilt in the lower grooves, causing the evaporator bubbles to compress in the lower grooves and thus increasing

the performance.

The percentage degradation in grooved pipes is seen to be relatively small compared to composite and arterial wicks (References 1 and 2). This relatively low degradation is attributed to only a small portion of the transport bubbles reaching the occlusion formed at the evaporator end, due to bubble mobility in the groove which allows the bubble to move into areas of vaporization and be purged into the vapor space.

5.2 STEADY STATE CONTROL TEST

For the control tests, the VCHP and the test fixture were installed in the thermal vacuum test chamber. The tests consisted of setting the sink temperature, the heat load, and the control point temperature. This provided data on the reservoir temperature, which was then correlated to the analytical predictions.

The maximum defined heat loads are shown in Figure 3-1, which show the maximum radiator heat rejection as a function of controller set point temperature. The minimum heat load was defined experimentally as the heat leak occurring when the radiator is exposed to the minimum sink temperature and the adiabatic section completely blocked. For experimental purposes, the minimum heat leak was determined by allowing the reservoir to attain a temperature equal to the vapor temperature and finding the heat load required to maintain a particular controller set point temperature. These results are shown in Figure 5-5. At 0°C, the heat leak is about 2.4 watts, compared to the predicted value of about 1.2 watts. The measured heat load was expected to be higher because of diffusion heat transfer.

At 30°C, the heat leak is about 7.9 watts, compared with a predicted value of 1.7 watts. A value between 2 watts and 3 watts was expected. The discrepancy is believed due to reservoir superheat. The reservoir thermocouple location was in the center of the inboard reservoir end cap. This temperature read about 26°C whereas the temperature at the reservoir-feeder tube weld was 13.9°C. Also, a significant heat leak was observed from the reservoir to the condenser section of the pipe. The thermocouple on the end of the condenser was up about 50°C from those in the middle, indicating

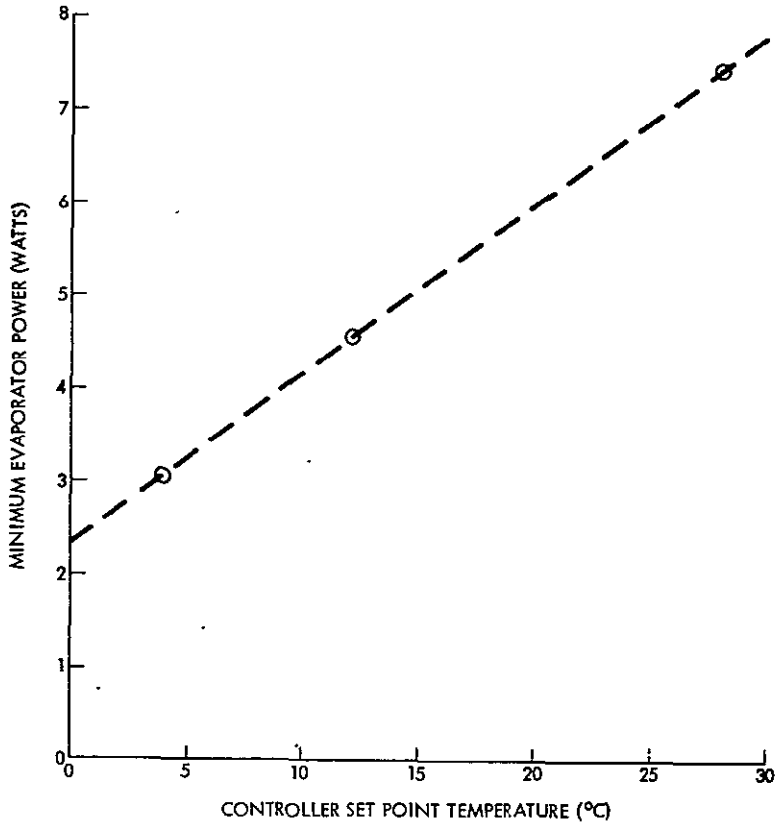

Figure 5-5 Experimental Minimum Power

that the reservoir volume is too small. The reservoir superheat is believed to be the major contributor to the high minimum heat load, but it is speculated that a smaller contributor was the low non-condensible gas concentration in the adiabatic section which increases diffusion heat transfer.

Once the minimum heat load curve was generated, the control tests were performed at 0°C and 30°C. Figure 5-6 shows the predicted minimum reservoir temperatures for the reservoir at -13°C and maximum heat load. The data points obtained for the -13°C and -120°C sink temperatures are also shown in Figure 5-6. Both of the -13°C data points are above the predicted values. From analytical considerations, these minimum reservoir temperatures were expected to be at or below the predicted values. There are two possible explanations for these results. First, the pipe is slightly undercharged with gas and therefore the design set point temperature is slightly below 0°C.

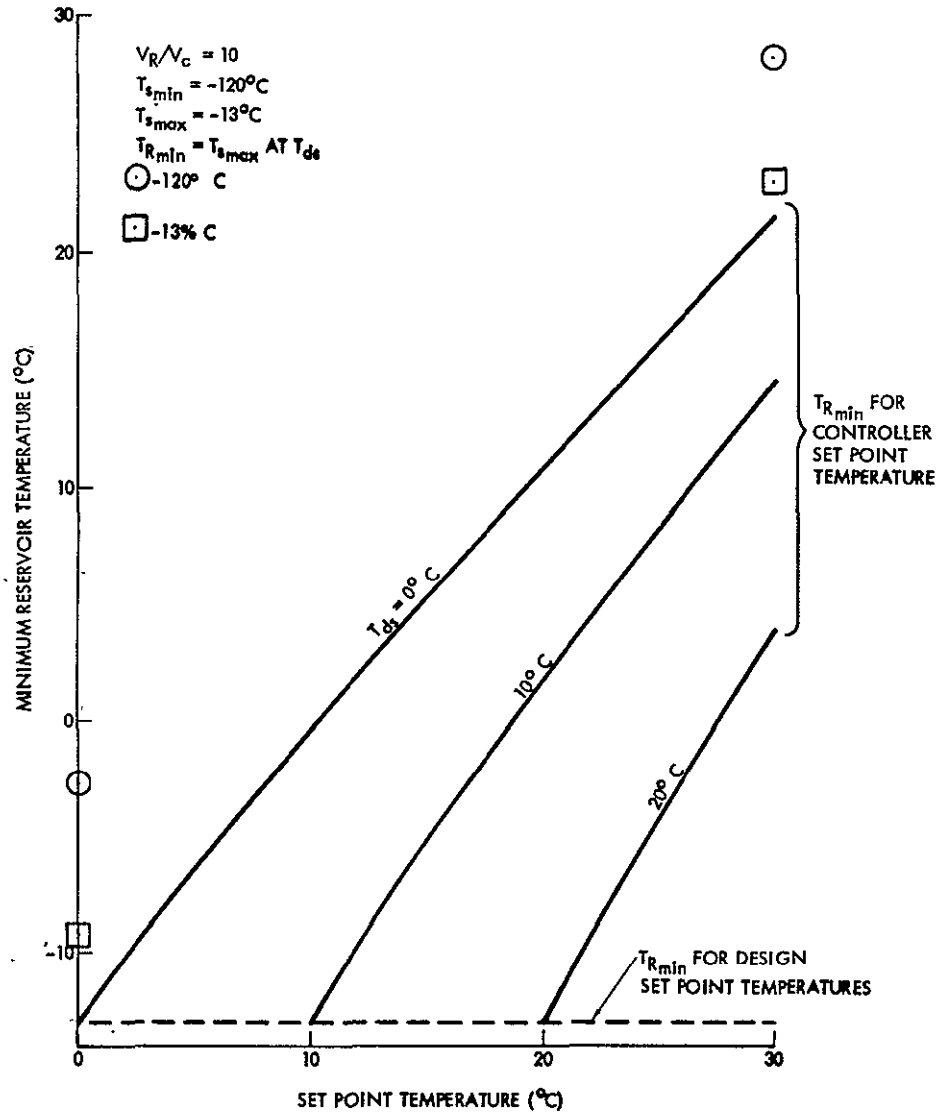

Figure 5-6 Minimum Reservoir Temperature Map

This is partially true, since the calculated curve assumes a minimum reservoir temperature of -10.2°C. If the minimum reservoir temperature were assumed to stabilize at -10.2°C (minimum reservoir temperature for -13°C sink, Figure 5-6); then the reservoir temperature is 1.8°C high. This shows that a small error in gas inventory is possible. The other explanation is superheated vapor at the reservoir thermocouple location. When heater power is applied to the reservoir, it is probable that the vapor in the upper portion of the reservoir becomes super-heated as a result of reservoir wick dry-out. Evidence of this was apparent in some tests, which showed the reservoir thermocouple in the center of the inboard end cap to be about 13°C above that of the thermocouple at the reservoir-feeder tube weld. Unless the temperature is sensed near the bottom of the reservoir, there exists the possibility of sensing a super-heated reservoir temperature. Figure 5-7 shows the predicted values of the maximum reservoir temperatures along with the experimental data. These curves were calculated for a sink temperature of -120°C. The measured value for the -120°C sink is 7.5°C above the predicted value. The heat conduction away from the reservoir is higher than it would be under space sink conditions resulting in a higher reservoir heater power and this high reservoir heater power could certainly produce the reservoir superheat problem mentioned above.

At 30°C, the reservoir temperature (center of inboard end cap) is equal to the vapor temperature, resulting in heat transport by vaporization from the reservoir to the condenser. This is clearly seen in the temperature profile of the condenser at the reservoir end, where the temperature increase was about 50°C. This is an indication that the reservoir volume is too small for control from 0°C to a 30°C controller set point temperature.

During the test program, one additional observation was made that could pose a potential start-up problem. This occurs when the condenser has been at the minimum sink temperature for a long time. All of the working fluid in the condenser is frozen, and it is desired to raise the controller set point temperature to 30°C by raising the reservoir temperature. The working fluid is vaporized in the reservoir and then condensed and frozen in the condenser section. When all of the working fluid in the reservoir is vaporized, then

the vapor in the reservoir is replaced by gas diffusing back into the reservoir. This causes the control point temperature to drop. This process was verified during test by reducing the reservoir temperature and allowing some of the vapor to condense back in the reservoir. The reservoir temperature was again raised and the controller set point temperature began to rise. When the reservoir fluid had vaporized, then the controller set point temperature began to fall again.

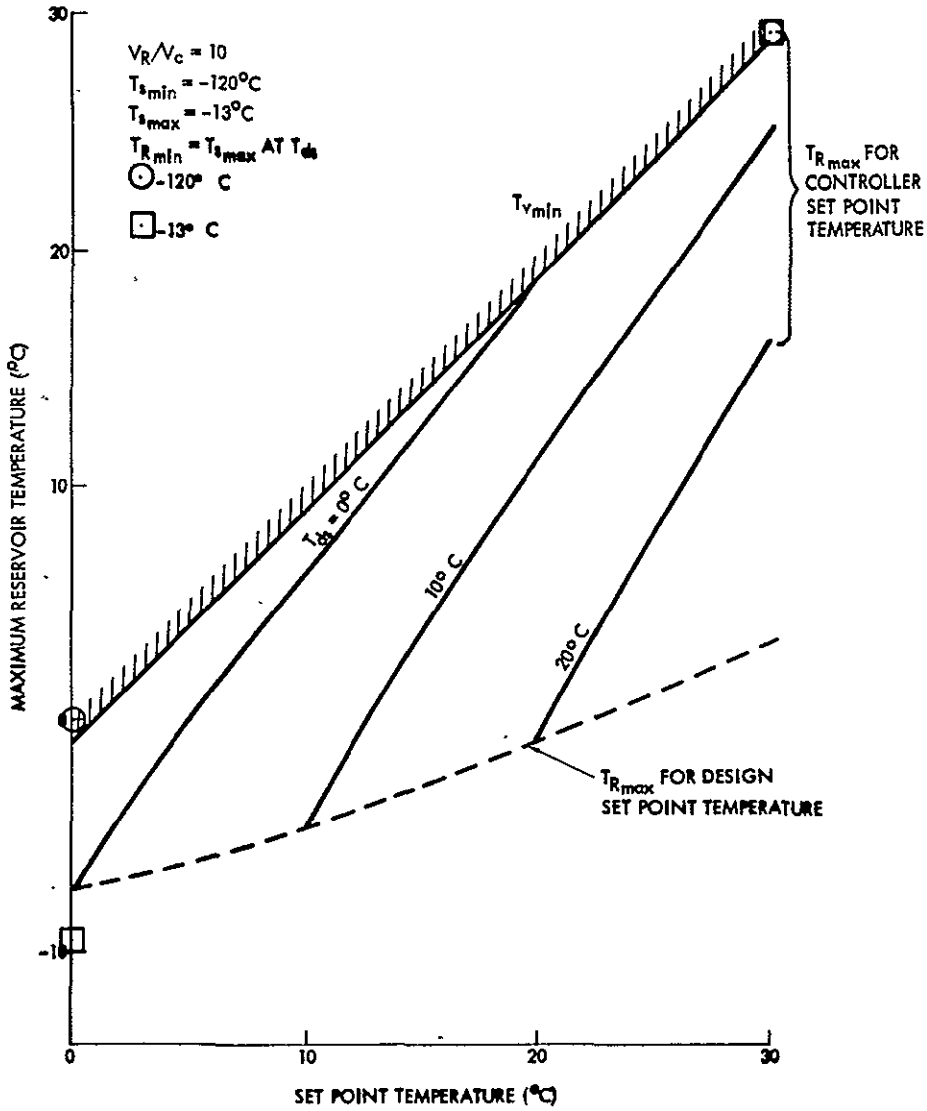

Figure 5-7 Maximum Reservoir Temperature Map

5.3 TRANSIENT TEST

For the transient test, a proportional controller was connected to the reservoir heater. At 0°C the VCHP was subjected to a step function that went from near worst case hot to near worst case cold, and then back to near worst case hot.

During the transfer from worst case hot (-13°C sink, 7.0 watts power) to worst case cold (-120°C sink, 4.0 watts power), the control point temperature went from 0.8°C to -2.2°C and finally stabilized at -2.0°C. It was subsequently determined that the simulated reservoir sink temperature was too cold. When the evaporator power was increased from 4 watts to 5 watts and the reservoir sink temperature was adjusted, the reservoir temperature began to rise, which caused the controller set point temperature to rise. Figure 5-8 shows that the maximum excursion from the stabilized temperature was about -0.2°C, as well as the slow increase in controller set point temperature after evaporator power and sink temperature were increased.

A maximum of 12 watts was available to the reservoir heater, but some of this power was dissipated to the lower sink temperature. Figure 5-8 shows that high reservoir heater power can be used to a certain extent to maintain the control point within the temperature tolerance band. A control point temperature profile similar to that shown in Figure 5-8 can be expected when the proper reservoir sink temperature is used, in which case a small control point temperature excursion outside the tolerance band may still exist.

The step change return to the worst hot case shows (Figure 5-8) that a temperature excursion of about 2.2°C above the tolerance band occurred. This is due to an overheated reservoir due to the step change. This overshoot could be significantly decreased by including a reservoir temperature limiting switch in the reservoir heater circuit.

At the 30°C set point temperature, the VCHP was again subjected to the change from worst case hot (-13°C sink; 25 watts power) to the worst case cold (-120°C sink; 78 watts power). An attempt was made to alleviate the problems associated with simulation of the radiation sink by increasing the reservoir heater power to about 30 watts. This however, led to further problems. Figure 5-9 shows that the control point temperature was maintained within the toler-

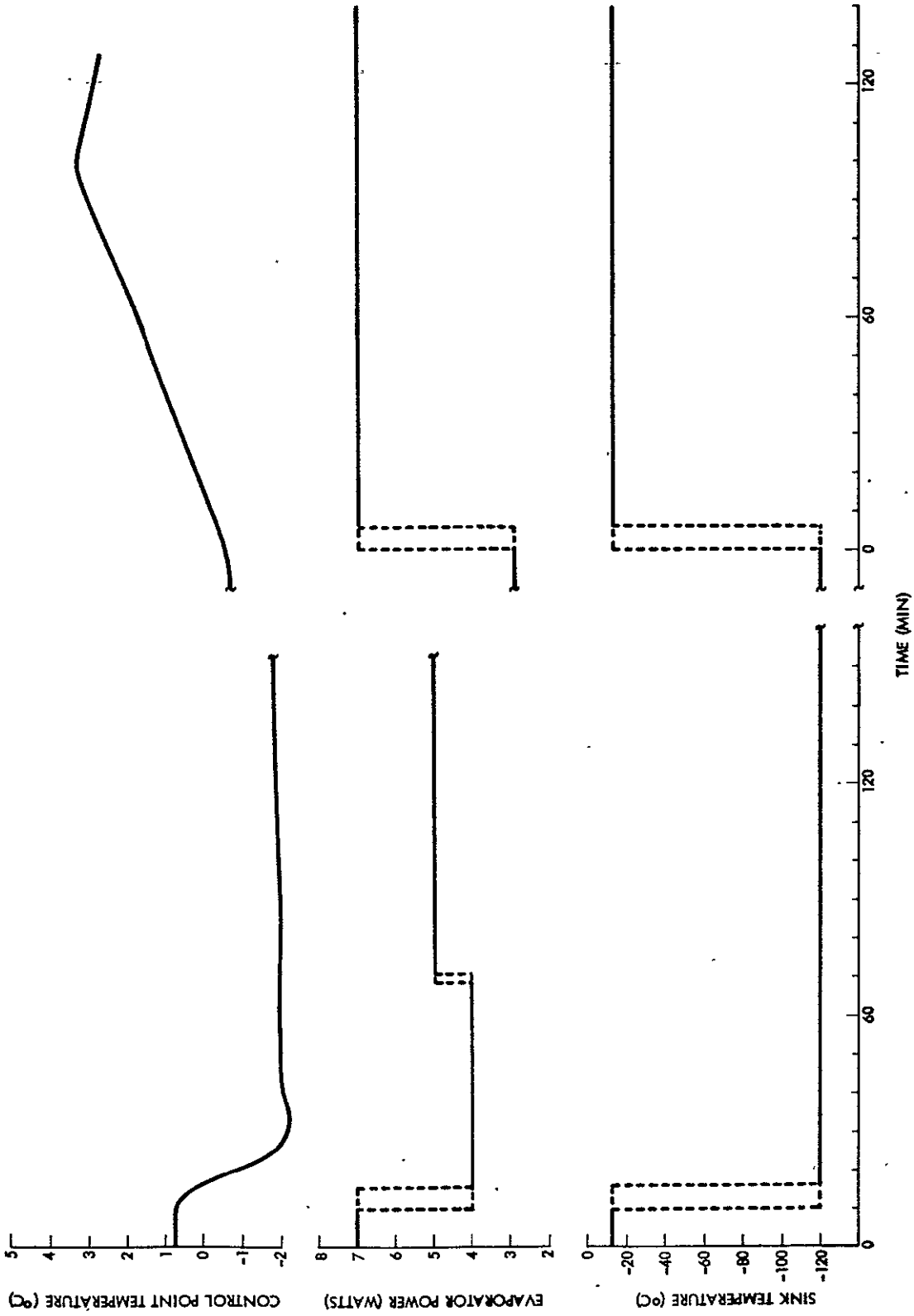

Figure 5-8 Transient Response from Worst Case Hot to Worst Case Cold to Worst Case Hot at 0°C.

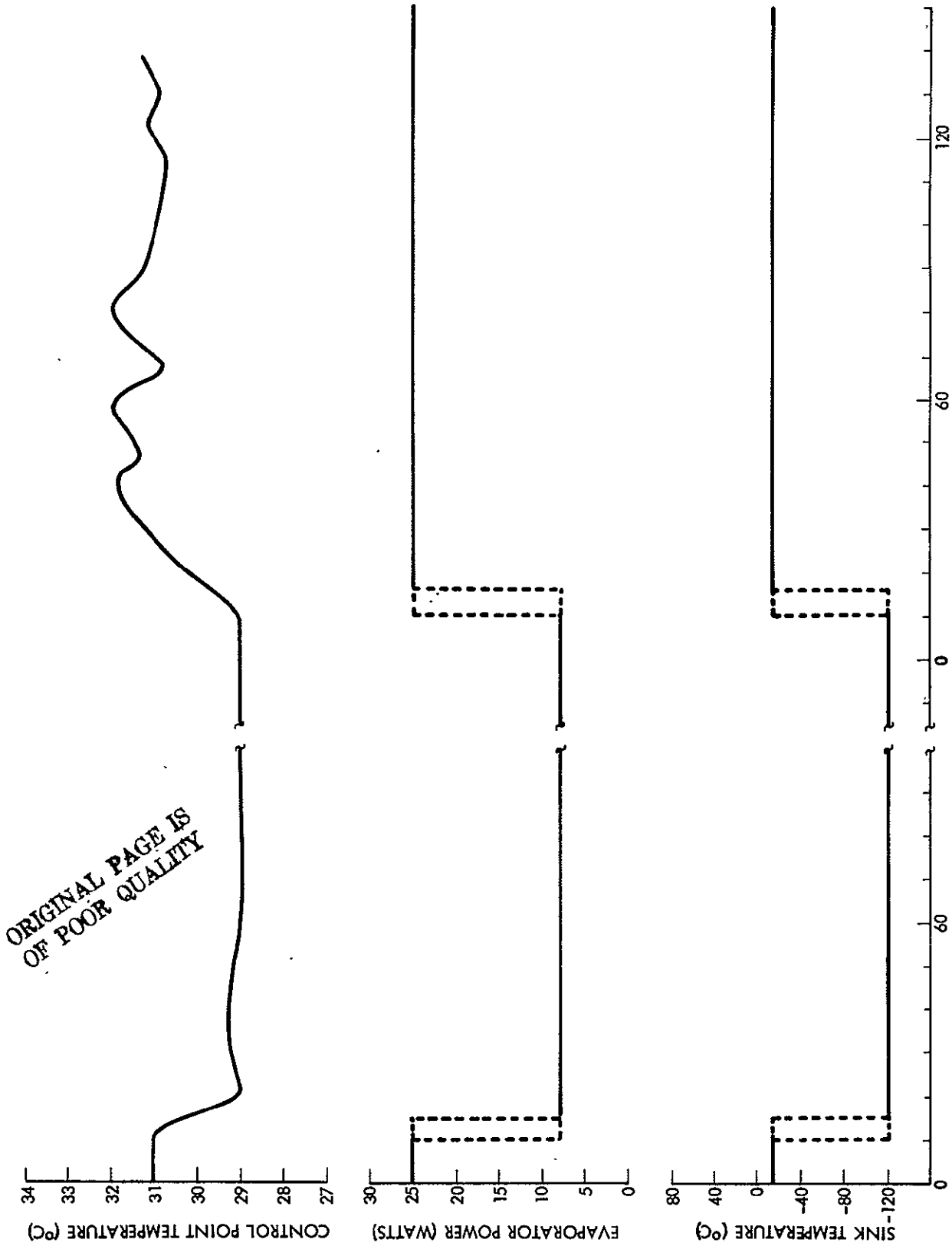

Figure 5-9 Transient Response from Worst Case Hot to Worst Case Cold to Worst Case Hot at 30°C

ance band as a result of the high reservoir heater power. However, there is reason to believe that the control point temperature would under-shoot the tolerance band if reasonable reservoir heater power were used, since the temperature profile observed in the condenser indicates a significant heat leak from the reservoir. Therefore, for reasonable size reservoir heaters, maintenance of control point temperature within the tolerance band may not be possible (for constant overall system dynamics), for the worst case cold condition at the 30°C controller set point.

For the step change back to the worst case hot condition, the controller was overridden by manually turning the heater on and off. This limited the maximum control point temperature overshoot to 1.0°C above the tolerance band. Originally, the reservoir temperature was maintained near the value it had when the system was stable at the worst cold condition, and allowed to cool only after overshoot began. The oscillations were due to the manually controlled heating and the cooling of the reservoir. If the reservoir were allowed to cool to the minimum reservoir temperature immediately, and if tighter reservoir temperature constraints were imposed then even less overshoot would occur.

6.0 CONCLUSIONS

A variable conductance heat pipe using feedback control was designed, manufactured, and tested to determine the heat transport limits, the steady state control characteristics, and the transient response characteristics. The heat transport capability was greater than or equal to the predicted values with no gas in the pipe. At 20°C, the transport at zero tilt was 160 watts, which exceeds the predicted value of 128 watts. When the pipe was tilted to .5 cm, the transport was 70 watts, as predicted.

When gas was added to the pipe, heat transport was degraded by 18% at zero tilt and 43% at .5 cm tilt. This degradation was expected and the data supports one hypothesis that a bubble occlusion is forming in the evaporator grooves.

During the control tests, an acceptable minimum heat load of 2.4 watts was observed at 0°C. However, with increasing set point temperatures, the measured minimum heat load was significantly above the predicted values. This result is believed due to superheated vapor in the reservoir, which led to erroneous reservoir temperature indications. This theory is supported by the temperature gradient measurements on the reservoir. The higher than predicted reservoir temperature in the control test was also due to the superheated vapor. Additional time and funds could alleviate this problem with the redesign of the reservoir heating and cooling system.

A potential start up problem was also isolated during the control tests and should be considered in future designs where freeze-out is possible. This problem occurs when fluid in the reservoir is vaporized and then frozen in the condenser, causing reservoir dryout and loss of control.

Transient response tests showed that maintenance of the control point temperature within the 0°C set point tolerance band is an attainable goal. At the 30°C set point, control was maintained with high heater power. Analysis shows that control cannot be maintained within the tolerance band and it is believed that tests using reasonably low heater powers will not maintain

control. Support of this conclusion was the observation of a substantial heat leak from the reservoir to the condenser. This heat leak also supports the analytical conclusion that the reservoir was slightly undersized for a controller set point temperature range of 0-30°C.

7.0 RECOMMENDATIONS

A number of design recommendations have been formulated from these tests. The primary recommendations are:

- Increase reservoir volume to a minimum V_R/V_c of 13.6
- Place reservoir heater as close to the feeder tube as possible.
- Improve reservoir wick transport capability.
- Improve reservoir sink temperature simulation.

NOMENCLATURE

A	-	Area
A'	-	Film coefficient area per unit length
A_{cs}	-	Cross sectional area of adiabatic section
A_{rad}	-	Radiator area
C	-	Capacitance
D	-	Diameter
K	-	Conductance; permeability
L	-	Section length
N_{ℓ}	-	Liquid transport factor
P	-	Perimeter
$P(T_a)$	-	Vapor pressure at temperature T_a
$P\{T_a\}$	-	$[P(T) - P(T_a)]$ at specified conditions
Re	-	Reynolds Number
$\dot{Q}$	-	Heat transfer rate
$\dot{Q}_{div}$	-	Heat leak with $\alpha = 0$ and $\beta = 1$
T	-	Temperature
V	-	Volume
f	-	Friction factor
$f(a_1, a_2, ---, a_n)$	-	function of variables a_1 through a_n
g	-	Acceleration of Gravity
h	-	Film coefficient of heat transfer; tilt
k	-	Thermal conductivity
n	-	Moles of non-condensable gas
r_p	-	Pore radius
s	-	Groove depth
ω	-	Groove width
Δ	-	Difference operator
α	-	$(L_b - L_c)/L_a$ @ cold case conditions; Groove half angle

α' – $(L_b - L_c)/L_a$ @ hot case conditions

β – L_b/L_c @ cold case conditions

β' – L_b/L_c @ hot case conditions

δ – Temperature tolerance

ε – Emissivity

η – Gravity factor, $\Delta P_b/\Delta P_c$

η_f – Radiator fin efficiency

η_{rad} – Radiator off efficiency

Θ – Contact Angle

Θ_1 – Slowest response time

Θ_2 – Fastest response time

λ – Heat of vaporization

μ – Absolute viscosity

ν – Kinematic viscosity

ρ – Density

σ – Stefan-Boltzmann constant; surface tension

ϕ – V_a/V_c

Subscripts

a – Adiabatic; dummy subscript

b – Body force

c – Condenser; cooling, capillary

ccx – Cooling @ $T_{cs\ max}$

cd – Cooling @ T_{ds}

ce – Control point to evaporator

cs – Control set point

ds – Design set point

e – Evaporator

eff – Effective

ev – Evaporator to vapor

h – Reservoir heater; heating; hydraulic

hcx - Heating @ $T_{cs\ max}$

hd - Heating @ T_{ds}

hvmcx - Heating to $T_{v\ min}$ @ $T_{cs\ max}$

ℓ - Liquid

ℓv - Liquid-vapor interaction

max - Maximum conditions

min - Minimum conditions

R - Reservoir

Rmcx - Minimum reservoir temperature @ $T_{cs\ max}$

Rmd - Minimum reservoir temperature @ T_{ds}

Rxcx - Maximum reservoir temperature @ $T_{cs\ max}$

Rxd - Maximum reservoir temperature @ T_{ds}

rad - Radiator

rs - Radiator to space

s - Effective sink conditions

v - Vapor

vr - Vapor to radiator

vs - Vapor space

ω - Wick

REFERENCES

1. Abhat, A., M. Groll, and M. Hage. Investigation of Bubbles Formation in Arteries of Gas-Controlled Heat Pipes. AIAA Paper No. 75-655 May, 1975.

2. Analysis and Test of NASA Covert Groove Heat Pipe, Grumman Aerospace Corporation, NASA CR-135156 (December 1976)

3. Bahr, A., E. Burch, and W. Hufschmidt, Liquid-Vapor Interaction and Evaporation in Heat Pipes, Paper D-6, 2nd International Conference on Thermionic Electric Power Generation, May 27-31, 1968.

4. Bienert, W. B. and P. Brennan, Feedback Controlled Variable Conductance Heat Pipes, AIAA Paper No. 71-421, 1971.

5. Definition of a Shuttle Thermal Canister Experiment, SD 76-SA-0150, December 1976.

6. Groll M., and M. Hage, Development of an Electrical Feedback Controlled Variable Conductance Heat Pipe for Space Application. AIAA Paper No. 74-752, July 1974.

7. Hildebrand, J. and R. Scott, The Solubility of Nonelectrolytes, Reinhold Publishing, N.Y. (1950).

8. Hirschfelder, C. Curtiss and R. Bird. Molecular Theory of Gases and Liquids, John Wiley and Sons, 1965.

9. Kroliczek, E. J. and P. Brennan. Axial Grooved Heat Pipes - Cryogenic Through Ambient. ASME Paper No. 73-ENAs-48, July 1973.

10. Lehtinen, A. Controllability Analysis for Passively and Actively Controlled Heat Pipes. AIAA Paper No. 77-776, June 1977.

11. Marcus, B. D. Theory and Design of Variable Conductance Heat Pipes. NASA CR-2018 (April 1972).

12. Schlitt, R., et al. Parametric Performance of Extruded Axial Grooved Heat Pipes from 100 to 300°K. AIAA Paper No. 74-724, July 1974.

13. Saaki, E. W. Heat Pipe Temperature Control Utilizing a Soluble Gas Absorption Reservoir. Sigma Research, Inc., NASA CR-137792 (February 1976).

14. Saaki, E. W. Investigation of Arterial Gas Occulations. NASA CR-114731, McDonnell Douglas Company, Washington, March 1974.

15. Saaki, E. W. Investigation of Bubbles in Arterial Heat Pipes. NASA CR-114531, McDonnell Douglas Company, Washington, December 1972.

16. Thermal Investigation and Analytical Modeling of Heat Pipe Thermal Interface Techniques, SD 73-SA-0086, June 1973.

17. Transient Thermal Response of a Thermal Control Canister. Grumman Aerospace Corp., Contract NAS5-22570 (1976).

18. Welty, J., C. Wicks, and R. Wilson. Fundamentals of Momentum, Heat and Mass Transfer. New York. John Wiley & Sons, Inc. (1969).

19. Wright, J. P. Heat Pipe Technology, Final IR&D Report for CFY 1975, Space Division Rockwell International, SD 75-SA-0200, (December 1975).